Full-duplex Reflective Beamsteering Metasurface Featuring Magnetless Nonreciprocal Amplification

Sajjad Taravati (sajjad.taravati@utoronto.ca)
University of Toronto https://orcid.org/0000-0003-3992-0050

George Eleftheriades
University of Toronto

Article

Keywords: electromagnetic wave radiation, nonreciprocal radiation

Posted Date: January 21st, 2021

DOI: https://doi.org/10.21203/rs.3.rs-139662/v1

Version of Record: A version of this preprint was published at Nature Communications on July 20th, 2021. See the published version at https://doi.org/10.1038/s41467-021-24749-7.

Full-duplex Reflective Beamsteering Metasurface Featuring Magnetless Nonreciprocal Amplification

Sajjad Taravati [1] and George V. Eleftheriades [1]

[1] *The Edward S. Rogers Sr. Department of Electrical and Computer Engineering, University of Toronto, Toronto, Ontario M5S 3G4, Canada*

Email: sajjad.taravati@utoronto.ca

Nonreciprocal radiation refers to electromagnetic wave radiation in which a structure provides different response under the change of the direction of the incident field. Modern wireless telecommunication systems demand versatile apparatuses which are capable of full-duplex nonreciprocal wave processing and amplification, especially in the reflective state. Here, we propose full-duplex reflective beamsteering metasurfaces for magnetless nonreciprocal wave amplification. To realize such a unique, extraordinary and versatile functionality, we propose a completely new architecture in which a chain of series cascaded radiating patches are integrated with nonreciprocal phase shifters, providing an efficient mechanism for wave reception, signal amplification, nonmagnetic nonreciprocal phase shifting and steerable wave reflection. Having accomplished all these functionalities in the reflective state, the metasurface represents a conspicuous apparatus for efficient, controllable and programmable wave engineering for wireless telecommunications. Such an ultrathin reflective metasurface can provide directive and diverse radiation beams, and steerable beams by simply changing the bias of the gradient active nonmagnetic nonreciprocal phase shifters.

The proposed structure provides large wave amplification and is immune to undesired time harmonics, yielding a highly efficient full-duplex reflective beamsteering apparatus.

1 Introduction

Over the past decade, the advent and development of metasurfaces has led to significant advances to wave processing in modern telecommunication and optical systems[1–14]. However, conventional static metasurfaces are restricted by the Lorentz reciprocity theorem which significantly limits their applications as versatile wave shapers and wave processors in modern wireless communication systems. Ferrite-based magnetic materials have been used for nonreciprocity implementation but they are cumbersome, costly, are not compatible with printed circuit board technology, and are not suitable for high frequency applications and future generation telecommunication systems. It is an object of this study to overcome some of the above-noted disadvantages. Lately, there has been a substantial scientific attraction to magnetless active metasurfaces for nonreciprocal wave processing[8,12,14–17]. Magnet-free nonreciprocal metasurfaces provide huge degrees of freedom for arbitrary alteration of the wavevector and temporal frequency of electromagnetic waves[8,12,14–23,23–25]. They may be classified into two main categories, that is, space-time metasurfaces[12,17,19,21,21,23,25–29] and transistor-loaded metasurfaces[8,15,30–32,32–34]. Among these nonreciprocity approaches, transistor-based nonreciprocity is of high interest thanks to its immense capability for efficient nonreciprocal electromagnetic-wave amplification while breaking the time reversal symmetry.

Active metasurfaces provide huge degrees of freedom for arbitrary and unidirectional alteration of the wavevector and amplitude of electromagnetic waves[8,12,16,19,19–24,35]. They represent

a class of compact dynamic wave processors for extraordinary transmission of electromagnetic waves. Reflective active metasurfaces represent a class of metasurfaces for simple and advanced wave tailoring [19,21,23,27,30,31,33,36]. They can be installed on a wall or inside a device like a cell phone or a laptop to provide a diverse range of wave engineering.

This paper proposes a low-profile reflective metasurfaces for nonreciprocal wave engineering and electromagnetic wave radiation control. The proposed reflective metasurface is capable of providing full-duplex unidirectional wave amplification and beam-steering. We introduce an original metasurface architecture in which a chain of series cascaded radiating patches are integrated with nonreciprocal phase shifters, providing an efficient mechanism for wave reception, unilateral signal amplification, nonmagnetic nonreciprocal phase shifting and steerable wave reflection. Such a unique, extraordinary and useful functionality has not been reported previously and is expected to find various applications in modern telecommunication systems. We provide the theory, simulation and experimental results of full-duplex nonreciprocal-beam-steering and wave amplification of these reflective metasurfaces. Such metasurfaces may be placed on a wall, thereby amplifying, transforming and directing the radiation pattern of a source antenna or a received wave non-reciprocally, while providing different radiation beams for the reception and reflection states. Such metasurfaces are composed of chains of transistor-based nonreciprocal phase shifters interconnected to antenna elements.

The proposed apparatus may be placed on a wall or in front of an antenna to amplify a wave, and/or steer a beam to a desired direction, i.e., transform the radiation pattern and introduce

different radiation patterns for waves incident from its left and right sides. The metasurface is endowed with directive, diverse and asymmetric reflection and reception radiation beams, and tunable beam shapes. Furthermore, these beams can be steered by changing the DC bias of the novel nonreciprocal phase shifters. Moreover, there is no undesired harmonics, yielding a high conversion efficiency with significant wave amplification which is of paramount importance for practical applications such as point to point full-duplex communications.

2 Operation Principle

Figure 1 shows the realization of the proposed reflective transistor-based metasurface. The metasurface is formed by a set of phase-gradient cascaded radiator-amplifier-phaser supercells. The metasurface comprises a dielectric layer sandwiched between two conductor layers. The bottom conductor layer acts as the ground plane of the patch antenna elements and also includes the direct current (DC) signal patch of the unilateral circuits. The top conductor layer includes patch antenna elements, transistors, and phase shifters. The dielectric layer separates the two conductor layers from each other. Each supercell is formed by a patch antenna element, a phase shifter and a unilateral circuit. When an electromagnetic wave is received at the surface of the metasurface, the metasurface reflects a wave having an identical frequency to the frequency of the received wave but towards a desired direction in space.

The metasurface system comprises a dielectric layer interposed between two conductor layers. Each of the conductor layers is formed by a plurality of supercells embedded therein. Each

supercell in the plurality of supercells comprises a microstrip patch radiator in electrical connection with a phase shifter and a unilateral transistor-based amplifier. The transistor radio frequency (RF) circuit includes two decoupling capacitors, and the DC biasing circuit of the transistor includes a choke inductor, two bypass capacitors and one biasing resistor. A DC signal biases the transistors to create a gradient non-reciprocal phase shift profile.

Figure 2 sketches the high-level architecture of the proposed reflective beamsteering metasurface. The metasurface thickness is subwavelength. In the forward problem, denoted by "F", the incoming wave from the right side impinges on the metasurface under the angle of incidence θ_{i} which is inside the reception beam of the metasurface. The reception beam of the metasurface is governed by the gradient phase shifters in each supercell. Hence, the wave is received by the metasurface, acquires a power gain and is reflected at the desired angle of reflection $\theta_{\mathrm{r}}^{\mathrm{F}}$, instead of the reflection angle $\theta_{\mathrm{r}} = -\theta_{\mathrm{i}}$ corresponding to the specular angle for reflection in conventional surfaces. In contrast, in the backward problem, denoted by "B", the incoming wave from the left side impinges on the metasurface under the angle of incidence $-\theta_{\mathrm{i}}$ which is outside the reception beam of the metasurface. Therefore, the wave is not received by the metasurface and is reflected at the reflection angle $\theta_{\mathrm{r}}^{\mathrm{B}}$ without reflection gain. Therefore, at a given frequency and for symmetric wave incidences, where $\theta_{\mathrm{i}}^{\mathrm{B}} = -\theta_{\mathrm{i}}^{\mathrm{F}}$, the reflective metasurface introduces different, nonreciprocal and asymmetric radiation patterns for the forward and backward incidences, i.e.,

$$\theta_{\mathrm{r}}^{\mathrm{F}} \neq -\theta_{\mathrm{r}}^{\mathrm{B}}, \tag{1}$$

and

$$E^{\mathrm{F}} \neq E^{\mathrm{B}}, \qquad |E(\theta_{\mathrm{r}}^{\mathrm{F}})| > |E(\theta_{\mathrm{r}}^{\mathrm{B}})|, \tag{2}$$

Figure 3 describes the beamsteering mechanism, including wave incidence and reflection from the cascaded supercells of the metasurface in Figs. 1 and 2. Each chain is constituted by N interconnected supercells, each of which is formed by a radiating patch element characterized by the length L and phase shift ϕ_{p}, a unilateral transistor-based amplifier characterized by the transmission function T_{U} and the phase shift ϕ_{U}, and a gradient phase shifter characterized by the transmission function T_{ϕ_n} and phase shift ϕ_{n}, where $1 < n < N$. The incoming wave from the right side impinges on the metasurface under the angle of incidence θ_{i} which is inside the reception beam of the metasurface, governed by the gradient phase shifters in each supercell. The incident wave is received by the radiating patch elements upon different phases corresponding to the angle of incidence θ_{i}. Then, the received signal at the feeding ports of the patch elements may be written in terms of voltages as

$$V_{\mathrm{i},n} = \sum_{n=1}^{N} V_{0\mathrm{i},n} e^{i\beta(N-n)d\sin(\theta_{\mathrm{i}})}, \tag{3}$$

where β is the wavenumber of the incident wave, and d denotes the distance between two adjacent elements. The reflected electric field is expressed as

$$E(\theta_{\mathrm{r}}) = \sum_{n=1}^{N} V_{\mathrm{o},n} e^{i\beta nd\sin(\theta_{\mathrm{r}})}, \tag{4}$$

where $V_{\mathrm{o},n} = V_{\mathrm{i},n}.T_{\mathrm{U}}.T_{\phi_n}$. Hence, the reflected electric field reads

$$E(\theta_{\mathrm{r}}) = \sum_{n=1}^{N} V_{0\mathrm{i},n}.T_{\mathrm{U}}.T_{\phi_n} e^{i\beta d[(N-n)\sin(\theta_{\mathrm{i}})+n\sin(\theta_{\mathrm{r}})]}, \tag{5}$$

which demonstrates the effect of the incident angle θ_{i}, unilateral transistor-based amplifier transfer function T_{U} and the gradient phase shifters transfer function T_{ϕ_n} on the reflected field magnitude and the angle of reflection θ_{r}. We shall stress that, here $V_{0\mathrm{i},n}$ is different for forward and backward

wave incidences as the metasurface provides an asymmetric reception beam which is realized by uni-directional gradient phase shifters.

Figure 4 depicts a schematic of a chain of the interconnected supercells. Each supercell is composed of a patch antenna element, and a nonreciprocal phase shifter. The nonreciprocal phase shifters can be either one-way or two-way. A one-way nonreciprocal phase shifter is constituted of a unilateral device, e.g. a transistor-based amplifier, incorporated with a fixed phase shifter. The patch antenna elements are double-fed microstrip patch antennas to allow the flow of the reflection of power in the desired direction inside the metasurface. However, the first and last patch antenna elements are single-fed patches. The chain of the interconnected patches and nonreciprocal phase shifters behave differently with the incident waves from the right side and the left side.

For further development of the proposed metasurface and for achieving a more versatile structure, one may use a two-way nonreciprocal phase shifter and amplifier as illustrated in Fig. 5. Such a nonreciprocal phase shifter is formed by two power dividers, two unilateral transistor-based amplifiers, two fixed phase shifters, and four decoupling capacitors. The top and bottom phase shifters provide different phase shifts. The top and bottom amplifiers may provide equal amplification and isolation, in the forward and backward directions, respectively. The signal entering the structure from the left side goes through the upper arm, experiences amplification by the top amplifier and then passes through the top phase shifter. However, the signal entering the structure from the right side goes through the lower arm, experiences amplification by the bottom amplifier and then passes through the bottom phase shifter.

3 Experimental set-up

Figure 6 illustrates the detailed architecture of the fabricated reflective beamsteering metasurface. The top layer includes a set of chains of patches interconnected through one-way transistor-based gradient nonreciprocal phase shifters. The bottom conductor layer includes two metallic sheets, one acting as the RF grounding of the patch antennas, and the other one provides the DC bias of the transistors. The DC bias of the transistors is supplied to the bottom-right side of the top layer, transferred to the bottom layer through a via hole, and then supplied to each transistor through a via hole.

Figure 7(a) shows a photo of the fabricated reflective metasurface. The metasurface is formed by 30 patch antenna elements, i.e., 20 double-fed and 10 single-fed patch antenna elements, and 25 nonreciprocal phase shifters. Each nonreciprocal phase shifter includes a reciprocal transmission-line based phase shifter, a GAli-2+ transistor-based amplifier, two decoupling capacitors, an inductor and a bypass capacitor. A total number of 25 Gali-2+ unilateral transistor-based amplifiers, 25 choke inductors of 15 nH, 25 bypass capacitors of 100 pF and 50 decoupling capacitances of 3 pF are used. The metasurface is fabricated as a two-layer circuit, i.e., two conductor layers and one dielectric layer, made of Rogers RO4350 with 30 mils height.

The metasurface comprises a dielectric layer sandwiched between two conductor layers, formed by an array chain of supercells. Supercells are comprised of patch antenna elements and non-reciprocal tunable phase shifters. When an electromagnetic wave at a given frequency impinges on the metasurface, the metasurface amplifies the wave instantly and reflects the wave to a

desired direction, having an identical frequency to the frequency of the incident wave. The feeding line supporting the DC bias of the unilateral amplifiers is embedded inside the bottom conductor ground-plane layer. The specifications of the supercells may be varied via a DC signal to control the properties of the reflected wave, including the angle of reflection and the amplitude of the reflected wave. Each supercell comprises one reciprocal phase shifter, one unilateral transistor-based amplifier, one choke inductance, two decoupling capacitances, and one bypass capacitor. The choke inductance prevents leakage of the incident electromagnetic wave to the DC biasing path, and the decoupling capacitances prevent leakage of the DC bias to the RF path of the next supercell.

Figures 7(b) and 7(c) show a schematic diagram illustrating the experimental demonstration of the nonreciprocal radiation beam reflective metasurface. The measurement set-up consists of the fabricated reflective metasurface, an absorber for holding the metasurface, a vector network analyzer, a DC power supply and two horn antennas.

4 Nonreciprocal beamsteering

Figure 8 illustrates full-duplex operation in the proposed reflective nonreciprocal-beam metasurface. Here, the incoming wave from the right side impinges on the metasurface and reflects to the left side and is received by the main RX and TX port at the left side of the metasurface upon the angle of reception θ_{RX}. However, the transmitting wave from the main RX and TX port impinges on the metasurfaces and reflects under the reflection angle $\theta_{\mathrm{TX}} \neq \theta_{\mathrm{RX}}$ while experiencing a much

lower gain. As a result, the metasurface functions as a full-duplex nonreciprocal-beam apparatus, where simultaneous reflection and reception at different angles is achieved.

Figures 9(a) to 9(h) plot the full-wave simulation results illustrating the nonreciprocal reflective beamsteering mechanism of the proposed metasurface. Here, the reflection gain of the metasurface for forward wave incidence is set to 1 for the sake of presentation so that both incident and reflected waves can be seen. As we see in these figures, the metasurface introduces different angles of reflection for each angle of incidence.

Figure 10(a) plots the experimental results demonstrating the nonreciprocal full-duplex beam steering functionality for wave incidence from the angle of incidence of $+80$ degrees. For the forward problem, where the incident wave impinges on the metasurface from the right side, i.e., upon the angle of incidence of +80 degrees, the wave is being amplified, about 16.5 dB by the metasurface instantly and is reflected to the desired angle of reflection of -5 degrees. However, for the backward problem, where the incident wave impinges on the metasurface from the left side, i.e., upon the angles of incidence of -5 and -80 degrees, the wave is not amplified significantly. The nonreciprocal-beam full-duplex operation in Fig. 10(a) is as follows. The main port for the reception and reflection is placed at -5 degrees. As a result, a reflection gain of +7.8 dB from -5 to +32 is achieved. However, a reception gain of 16.2 dB is achieved from +80 to -5. Hence, the metasurface is capable of simultaneous reception and reflection but at different reception and reflection angles, i.e. with a reflection angle of +32 degrees and a reception angle of +80 degrees. Figure 10(b) plots the experimental results demonstrating the frequency response of the nonrecip-

rocal full-duplex beam steering functionality for wave incidence from the angle of incidence of 80 degrees. The isolation between the wave reflection at different angles shows that a proper wave amplification and isolation is achieved at the frequency of 5.81 GHz.

Figure 10(c) plots the experimental results demonstrating the nonreciprocal full-duplex beam steering functionality for wave incidence from the angle of incidence of $+70$ degrees. For the forward problem, where the incident wave impinges on the metasurface from the right side, i.e., upon the angle of incidence of +70 degrees, the wave is being amplified about 19 dB by the metasurface and is reflected to the desired angle of reflection of -20 degrees. However, for the backward problem, where the incident wave impinges on the metasurface from the left side, i.e., upon the angles of incidence of -20 and -70 degrees, the wave is amplified less than 13 dB and under angles of reflection corresponding to the opposite of angles of incidence. The nonreciprocal-beam full-duplex operation in Fig. 10(c) is as follows. The main port for the reception and reflection is placed at -20 degrees. As a result, a reflection gain of +12 dB from -20 to +20 degrees is achieved. However, a reception gain of 18.5 dB is achieved from +70 to -20 degrees. Hence, the metasurface is capable of simultaneous reflection and reception but at different reception and reflection angles, i.e. with a reflection angle of +20 degrees and a reception angle of +70 degrees. Figure 10(d) plots the experimental results demonstrating the frequency response of the nonreciprocal full-duplex beam steering functionality for wave incidence from the angle of incidence of 70 degrees. The isolation between the wave reflection at different angles shows that a proper wave amplification and isolation is achieved at the frequency of 5.81 GHz.

Figure 10(e) plots the experimental results demonstrating the nonreciprocal full-duplex beam steering functionality for wave incidence from the angle of incidence of 60 degrees. For the forward problem, where the incident wave impinges on the metasurface from the right side, i.e., upon the angle of incidence of +60 degrees, the wave is being amplified more than 21.2 dB by the metasurface instantly and is reflected to the desired angle of reflection of -28.5 degrees. However, for the backward problem, where the incident wave impinges on the metasurface from the left side, i.e., upon the angle of incidence of –28.5 and -60 degrees, the wave is not amplified significantly. Nonreciprocal operation of the metasurface is not only relevant to different wave amplification for forward and backward wave incidences, but also to angular beamsteering. The nonreciprocal beamsteering operation of the metasurfaces is as follows. For the forward problem, corresponding to the angle of incidence of +60 degrees, the ordinary reflection reads -60 degrees, but the wave is steered toward -28.5 degree according to the phase gradient profile of the metasurface. However, for the backward wave incidence, corresponding to the angle of incidence of -28.5 degree, the wave is reflected under the ordinary angle of reflection, i.e., +28 degrees. This is due to the fact that the nonreciprocal phase gradient profile of the metasurface mainly affects the forward waves coming from the right side. Figure 10(f) plots the experimental results demonstrating the frequency response of the nonreciprocal full-duplex beam steering functionality for wave incidence from the angle of incidence of 60 degrees. The isolation between the wave reflection at different angles shows that a proper wave amplification and isolation is achieved at the frequency of 5.81 GHz.

Figure 10(g) plots the experimental results demonstrating the nonreciprocal full-duplex beam steering functionality for wave incidence from the angle of incidence of 50 degrees. For the for-

ward problem, where the incident wave impinges on the metasurface from the right side, i.e., upon the angle of incidence of +50 degrees, the wave is being amplified, more than 21.7 dB, by the metasurface instantly and is reflected to the desired angle of reflection of -20 degrees. However, for the backward problem, where the incident wave impinges on the metasurface from the left side, i.e., upon the angle of incidence of -20 and -50 degrees, the waves are reflected approximately under ordinary angles of reflection and with much less power amplification. The nonreciprocal full-duplex operation in Fig. 10(g) is as follows. The main port for the reception and reflection is placed at -20 degrees. As a result, a reflection gain of +12 dB from -20 to +24 degrees is achieved. However, a reception gain of 21.6 dB is achieved from +50 to -20 degrees. Hence, the metasurface is capable of simultaneous reception and reflection but at different reflection and reception angles, i.e. with a reflection angle of +24 degree and a reception angle of +50 degrees. Figure 10(h) plots the experimental results demonstrating the frequency response of the nonreciprocal full-duplex beam steering functionality for wave incidence from the angle of incidence of 50 degrees. The isolation between the wave reflection at different angles shows that more than 21.7 dB wave amplification and isolation is achieved at the frequency of 5.81 GHz.

Next, we show the strong nonreciprocal amplification regime of the metasurface, where $\theta_{\mathrm{i}} < 45^{\circ}$. Here, more than 21 dB reflection gain for forward wave incidence is achieved while the backward reflection gain is less than 3dB. The metasurface is designed to present full amplification for $\theta_{\mathrm{i}} = 40^{\circ}$ corresponding to the normal reflection, i.e., $\theta_{\mathrm{r}} = 0^{\circ}$. Figure 11(a) plots the experimental results demonstrating the nonreciprocal full-duplex wave amplification functionality for wave incidence from the angle of incidence of 40 degrees. For the forward problem, where the

incident wave impinges on the metasurface from the right side, i.e., upon the angle of incidence of +40 degrees, the wave is being amplified, about 21.6 dB, by the metasurface instantly and is reflected to the desired angle of reflection of zero degree. However, for the backward problem, where the incident wave impinges on the metasurface from the left side, i.e., under the angle of incidence of -40 degrees, the wave is not amplified significantly.

Figure 11(b) plots the experimental results demonstrating the nonreciprocal full-duplex beam steering functionality for wave incidence from the angle of incidence of 45 degrees. For the forward problem, where the incident wave impinges on the metasurface from the right side, i.e., upon the angle of incidence of +45 degree, the wave is being amplified, more than 25 dB, by the metasurface instantly and is reflected to the desired angle of reflection of -18 degrees. However, for the backward problem, where the incident wave impinges on the metasurface from the left side, i.e., under the angle of incidence of -45 degree, the wave is not amplified significantly and is not beam-steered.

Table 1 lists a summary of the full-duplex nonreciprocal beamsteering reflective metasurface performance.

5 Programmable and Controllable Beamsteering

Figure 12(a) plots the experimental results demonstrating the beam steering functionality through changing the phase shift of the nonreciprocal phase shifters for wave incidence from the angle of incidence of +30 degrees at the frequency 5.8 GHz. For the forward problem, where the incident

wave impinges on the metasurface from the right side, i.e., upon the angle of incidence of +60 degrees, the wave is being amplified more than 10 dB by the metasurface instantly and is reflected to different desired angles of reflection for the DC bias of 3.7V and 3.84V.

Figure 12(b) plots the experimental results demonstrating the beam steering functionality through changing the phase shift of the nonreciprocal phase shifters, by the DC bias, for wave incidence from the angle of incidence of +60 degrees at 5.8 GHz. For the forward problem, where the incident wave impinges on the metasurface from the right side, i.e., upon the angle of incidence of +60 degrees, the wave is being amplified more than 10 dB, by the metasurface instantly and is reflected to different desired angles of reflection for the DC bias of 3.6V, 3.84V and 4V.

6 Near-Field Operation

Figure 13(a) shows a schematic representation of the near-field experimental set-up of the nonreciprocal radiation beam reflective metasurface. In this experiment, the two source horn antennas are placed inside the near-field zone of the metasurface and very close to the metasurface.

Figure 13(b) plots the experimental results demonstrating the near-field performance of the metasurface for wave incidence from the angle of incidence of +40 degrees. This figure shows that the metasurface provides very close results for both far-field and near-field experiments. This shows great performance of the metasurface in the near-field. Such a unique near-field performance, i.e, near-field wave amplification, nonreciprocity, and beam-steering, is expected to find numerous applications in 6G indoor wireless communications.

7 Discussion

The main concept of this paper is the realization of a reflective metasurface which is capable of *non-reciprocal beam* generation. Such a metasurface realizes full-duplex nonreciprocal-beamsteering and amplification in the reflective state where simultaneous reception and reflection of waves are accomplished but at different reflection angles, lacking any undesired frequency change and with distinct reception and reflection gains. This is totally different than other proposed nonreciprocal metasurfaces[16,21,27,34,37,38] in which the metasurface changes the spectrum of the incident wave and introduces an undesired frequency alteration. The recently proposed nonreciprocal reflective time-modulated metasurfaces[16,21,27,34,38] suffer from an unwanted frequency change in the spectrum of the incident wave, so that the reflected wave acquires a different frequency than the incident wave. Such a frequency change is very impractical as the frequency conversion ratio is very small so that one cannot achieve a practical frequency conversion functionality. However, in our proposed nonreciprocal-beam metasurface, the incident and reflected waves share the same frequency. Hence, the proposed metasurface is more practical. Furthermore, some of the recently proposed nonreciprocal metasurfaces are transmissive structures[8,12], which are not suitable for practical applications. In contrast, the proposed reflective metasurface in this study is very practical as it can be mounted on a wall and provide a desired beamsteering and amplification.

We have introduced a new architecture for reflective wave engineering comprising chains of patch antenna elements with embedded non-reciprocal amplifying phase shifters. This architecture is unique even in the case of traditional reciprocal reflect-arrays[39,40]. For the proposed

non-reciprocal reflective surface, there is no inherent limit to the bandwidth as the frequency bandwidth of the proposed unit cells can be easily enhanced through engineering approaches for the bandwidth enhancement of patch resonators[41,42].

In terms of applications, such metasurfaces can be elegantly mounted on a wall or on a smart device in a seamless way. These surfaces are capable of massive MIMO beam-forming, as no excessive RF feed lines and matching circuits are required, the metasurface functionality and operation can be fully controlled and programmed through biasing of unilateral devices and phase shifters, as well as tunable patch radiators. Highly directive and reflective full-duplex nonreciprocal-beam operation is a very promising feature of the proposed metasurface to be used for a low-cost high capability and programmable wireless beam-forming. The metasurfaces can become the core of an intelligent connectivity solution for signal enhancement in WiFi , cellular, satellite receivers and IoT sensors. It provides fast scanning between users while providing full-duplex multiple access and signal coding.

8 Conclusion

We have proposed a reflective metasurface that provides the opportunity to realize full-duplex reflection beamsteering accompanied by wave amplification. A mechanism is proposed to achieve nonreciprocal beam operation in the reflection state, such that the structure can be used as a radome for antennas or can be installed on a wall. The incident and reflected waves share the same frequency. The nonreciprocal phase and magnitude transitions in supercells are used to realize a radi-

ating nonreciprocal phase shifter, where the structure is immune to undesired frequency harmonics. The frequency bandwidth of the proposed supercells may be enhanced by using engineering approaches for the bandwidth enhancement of microstrip patch elements and nonreciprocal phase shifters. Given the strong capability of the proposed metasurface in both near-field and far-field wave amplification, nonreciprocity, and beam-steering, the structure is expected to find numerous applications in 6G and massive MIMO indoor wireless communications.

1. Yu, N. *et al.* Light propagation with phase discontinuities: Generalized laws of reflection and refraction. *Science* **334**, 333–337 (2011).

2. Wakatsuchi, H., Kim, S., Rushton, J. J. & Sievenpiper, D. F. Waveform-dependent absorbing metasurfaces. *Phys. Rev. Lett.* **111**, 245501 (2013).

3. Ni, X., Kildishev, A. V. & Shalaev, V. M. Metasurface holograms for visible light. *Nat. Commun.* **4**, 1–6 (2013).

4. Lin, D., Fan, P., Hasman, E. & Brongersma, M. L. Dielectric gradient metasurface optical elements. *science* **345**, 298–302 (2014).

5. Memarian, M. & Eleftheriades, G. V. Dirac leaky-wave antennas for continuous beam scanning from photonic crystals. *Nature communications* **6**, 1–9 (2015).

6. Zheng, G. *et al.* Metasurface holograms reaching 80% efficiency. *Nature nanotechnology* **10**, 308–312 (2015).

7. Epstein, A., Wong, J. P. & Eleftheriades, G. V. Cavity-excited huygens' metasurface anten-

nas for near-unity aperture illumination efficiency from arbitrarily large apertures. *Nature communications* **7**, 1–10 (2016).

8. Taravati, S., Khan, B. A., Gupta, S., Achouri, K. & Caloz, C. Nonreciprocal nongyrotropic magnetless metasurface. *IEEE Trans. Antennas Propagat.* **65**, 3589–3597 (2017).

9. Li, G., Zhang, S. & Zentgraf, T. Nonlinear photonic metasurfaces. *Nature Reviews Materials* **2**, 17010 (2017).

10. Asadchy, V. S., Díaz-Rubio, A. & Tretyakov, S. A. Bianisotropic metasurfaces: physics and applications. *Nanophotonics* **7**, 1069–1094 (2018).

11. Wang, X. *et al.* Extreme asymmetry in metasurfaces via evanescent fields engineering: Angular-asymmetric absorption. *Phys. Rev. Lett.* **121**, 256802 (2018).

12. Taravati, S. & Eleftheriades, G. V. Full-duplex nonreciprocal beam steering by time-modulated phase-gradient metasurfaces. *Phys. Rev. Appl.* **14**, 014027 (2020).

13. Wang, Z. *et al.* Three-dimensional microwave holography based on broadband huygens' metasurface. *Phys. Rev. Appl.* **13**, 014033 (2020).

14. Taravati, S. & Eleftheriades, G. V. Four-dimensional wave transformations by space-time metasurfaces. *arXiv:2011.08423 [physics.app-ph]* (2020).

15. Wang, Z. *et al.* Gyrotropic response in the absence of a bias field. *Proc. Natl. Acad. Sci. U.S.A.* **109**, 13194–13197 (2012).

16. Hadad, Y., Sounas, D. L. & Alù, A. Space-time gradient metasurfaces. *Phys. Rev. B* **92**, 100304 (2015).

17. Taravati, S. & Eleftheriades, G. V. Space-time medium functions as a perfect antenna-mixer-amplifier transceiver. *Phys. Rev. Appl.* **14**, 054017 (2020).

18. Taravati, S. Giant linear nonreciprocity, zero reflection, and zero band gap in equilibrated space-time-varying media. *Phys. Rev. Appl.* **9**, 064012 (2018).

19. Zhang, L. *et al.* Space-time-coding digital metasurfaces. *Nat. Commun.* **9**, 4334 (2018).

20. Taravati, S. & Kishk, A. A. Advanced wave engineering via obliquely illuminated space-time-modulated slab. *IEEE Trans. Antennas Propagat.* **67**, 270–281 (2019).

21. Zang, J. W. *et al.* Nonreciprocal wavefront engineering with time-modulated gradient metasurfaces. *Phys. Rev. Appl.* **11**, 054054 (2019).

22. Taravati, S. & Kishk, A. A. Dynamic modulation yields one-way beam splitting. *Phys. Rev. B* **99**, 075101 (2019).

23. Taravati, S. & Eleftheriades, G. V. Generalized space-time periodic diffraction gratings: Theory and applications. *Phys. Rev. Appl.* **12**, 024026 (2019).

24. Saikia, M., Srivastava, K. V. & Ramakrishna, S. A. Frequency-shifted reflection of electromagnetic waves using a time-modulated active tunable frequency-selective surface. *IEEE Trans. Antennas Propagat.* **68**, 2937–2944 (2019).

25. Taravati, S. & Kishk, A. A. Space-time modulation: Principles and applications. *IEEE Microw. Mag.* **21**, 30–56 (2020).

26. Taravati, S. & Caloz, C. Mixer-duplexer-antenna leaky-wave system based on periodic space-time modulation. *IEEE Trans. Antennas Propagat.* **65**, 442 – 452 (2017).

27. Guo, X., Ding, Y., Duan, Y. & Ni, X. Nonreciprocal metasurface with space-time phase modulation. *Light Sci. Appl.* **8**, 1–9 (2019).

28. Wu, Z., Scarborough, C. & Grbic, A. Space-time-modulated metasurfaces with spatial discretization: Free-space N-path systems. *Phys. Rev. Appl.* **14**, 064060 (2020).

29. Wang, X. *et al.* Nonreciprocity in bianisotropic systems with uniform time modulation. *arXiv* arXiv–2001 (2020).

30. Li, A. *et al.* High-power transistor-based tunable and switchable metasurface absorber. *IEEE Trans. Antennas Propagat.* **65**, 2810–2818 (2017).

31. Kang, L., Jenkins, R. P. & Werner, D. H. Recent progress in active optical metasurfaces **7**, 1801813 (2019).

32. Lončar, J., Grbic, A. & Hrabar, S. Ultrathin active polarization-selective metasurface at X-band frequencies. *Phys. Rev. B* **100**, 075131 (2019).

33. Taravati, S. & Eleftheriades, G. V. Programmable nonreciprocal meta-prism. *arXiv:2012.07525* (2020).

380 34. Cardin, A. E. *et al.* Surface-wave-assisted nonreciprocity in spatio-temporally modulated
381 metasurfaces. *Nat. Commun.* **11**, 1–9 (2020).

382 35. Taravati, S. & Eleftheriades, G. V. Perfect-frequency-converter metasurface consisting of twin
383 time-modulated radiators. In *IEEE AP-S Int. Antennas Propagat. (APS)* (Montreal, Canada,
384 2020).

385 36. Shi, Y. & Fan, S. Dynamic non-reciprocal meta-surfaces with arbitrary phase reconfigurability
386 based on photonic transition in meta-atoms. *Appl. Phys. Lett.* **108**, 021110 (2016).

387 37. Taravati, S., Chamanara, N. & Caloz, C. Nonreciprocal electromagnetic scattering from a
388 periodically space-time modulated slab and application to a quasisonic isolator. *Phys. Rev. B*
389 **96**, 165144 (2017).

390 38. Shi, Y., Han, S. & Fan, S. Optical circulation and isolation based on indirect photonic transi-
391 tions of guided resonance modes. *ACS Photonics* **4**, 1639–1645 (2017).

392 39. Berry, D., Malech, R. & Kennedy, W. The reflectarray antenna. *IEEE Trans. Antennas Prop-*
393 *agat.* **11**, 645–651 (1963).

394 40. Huang, J. Reflectarray antenna. *Encyclopedia of RF and Microwave Engineering* (2005).

395 41. Moradi, A. & Rahman, T. A. Broadband modified rectangular microstrip patch antenna using
396 stepped cut at four corners method. *Prog. Electromag. Res.* **137**, 599–619 (2013).

397 42. Bzeih, A., Chahine, S. A., Kabalan, K. Y., El-Hajj, A. & Chehab, A. An improved broadband
398 e patch microstrip antenna for wireless communications. *Radio Sci.* **42** (2007).

Acknowledgements This work was supported in part by TandemLaunch Inc. and LATYS, Montreal, QC, Canada, and in part by the Natural Sciences and Engineering Research Council of Canada (NSERC). The authors would like to especially thank Mr. Gursimran Singh Sethi, Co-founder and Technical Leader of LATYS, and Dr. Omar Zahr, Director of Technology at TandemLaunch Inc., for their great help and support.

Competing Interests The authors declare that they have no competing financial interests.

Correspondence Correspondence and requests for materials should be addressed to Sajjad Taravati (email: sajjad.taravati@utoronto.ca).

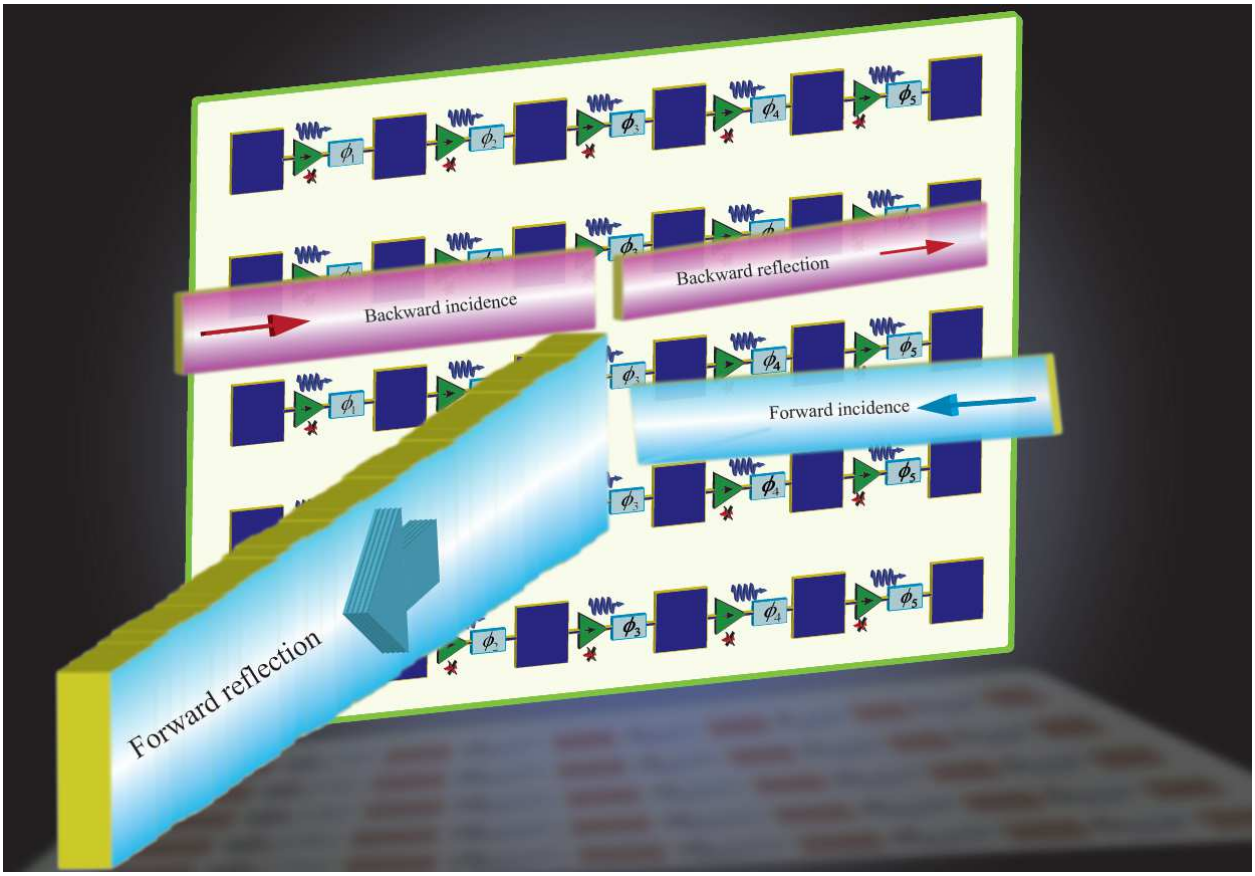

Figure 1: Schematic of the reflective beamsteering metasurface constituted of cascaded radiator-amplifier-phaser chains for simultaneous reflection and reception at different angles of reception and reflection.

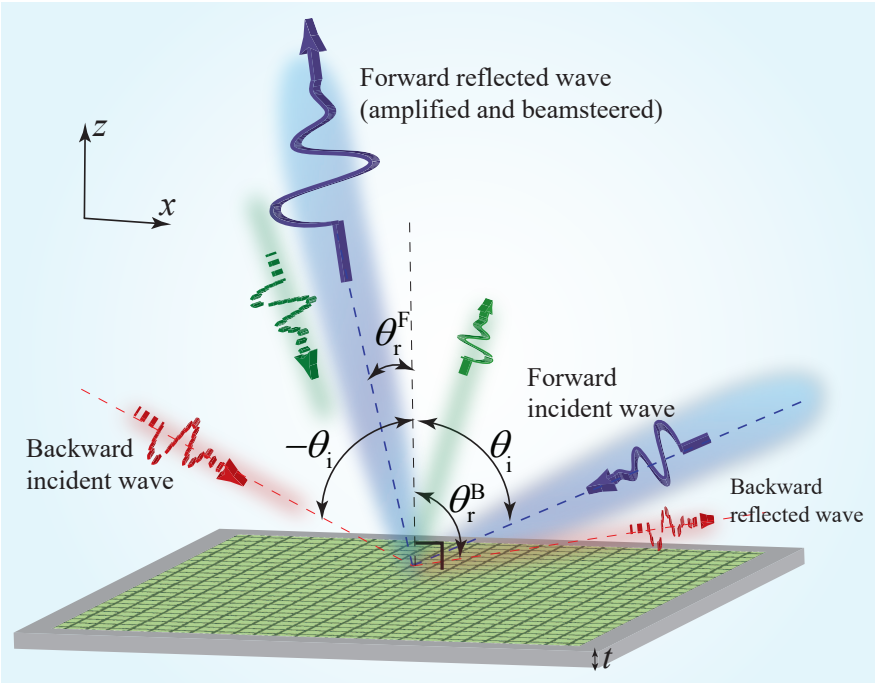

Figure 2: Functionality of the proposed reflective beamsteering metasurface.

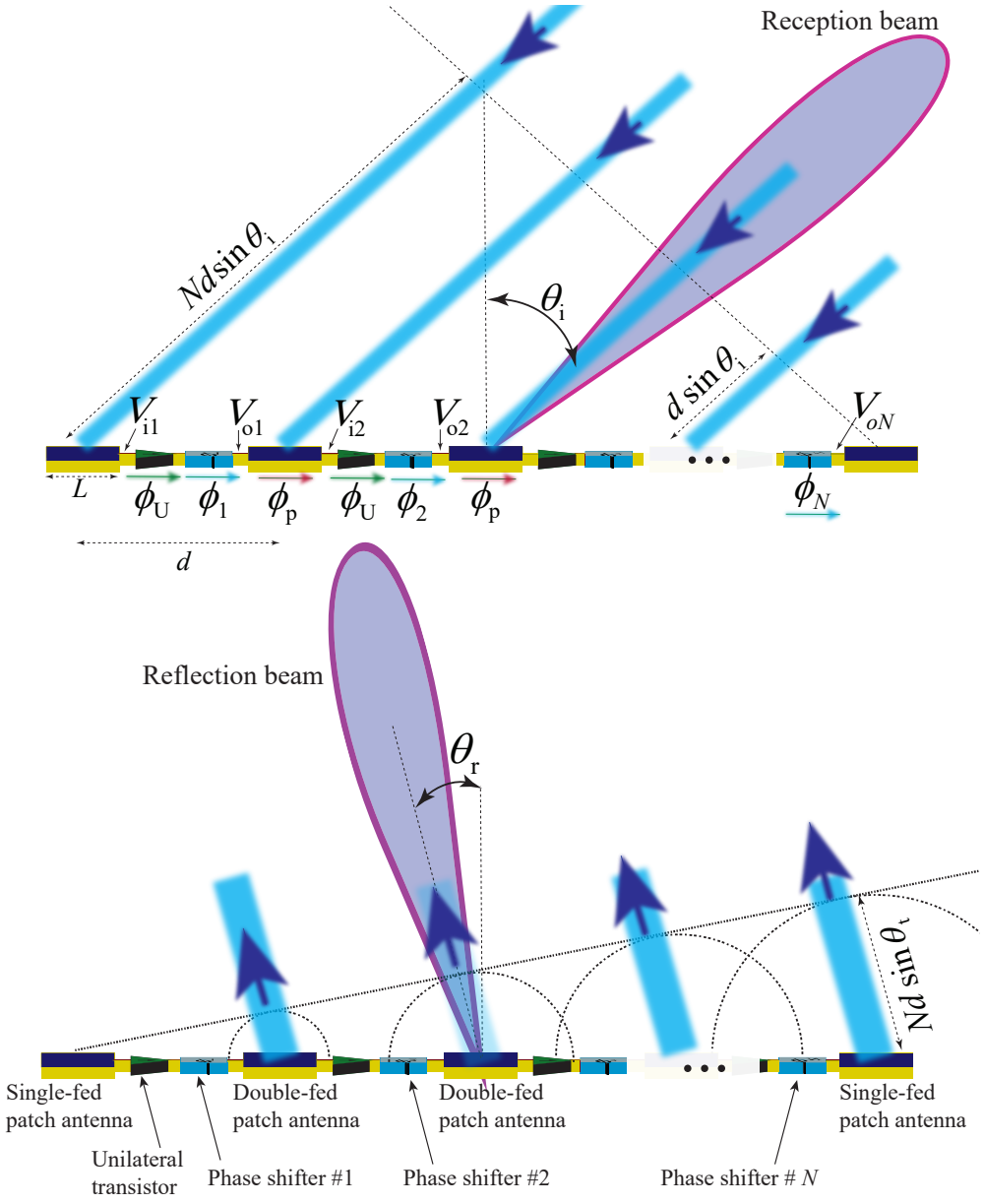

Figure 3: Beamsteering mechanism of the nonreciprocal reflective metasurface. A chain of series cascade radiating patches are integrated with nonmagnetic nonreciprocal phase shifters, providing an efficient mechanism for wave reception, one-way signal amplification, nonmagnetic nonreciprocal phase shifting and steerable wave reflection.

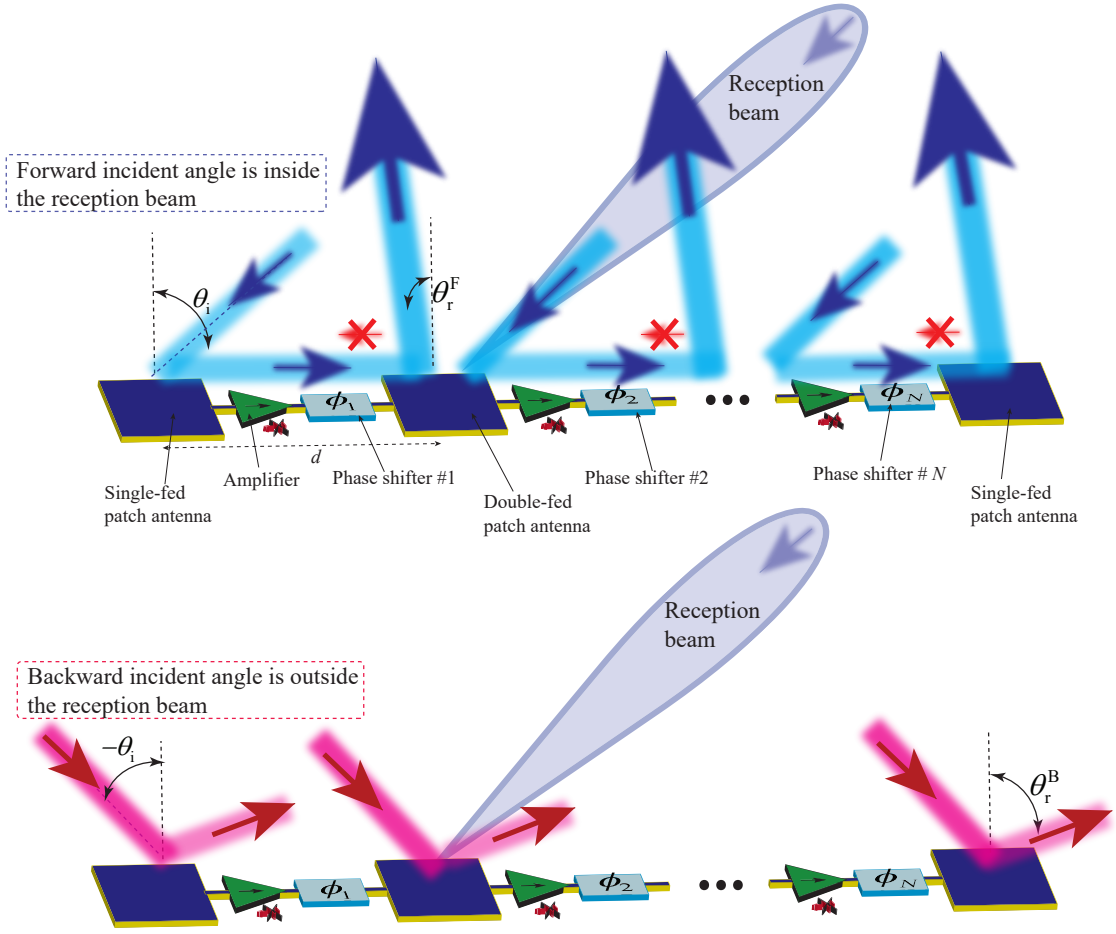

Figure 4: Nonreciprocity of the full-duplex reflective metasurface with an asymmetric reception beam governed by chains of series cascaded radiating patches integrated with phase shifters and unilateral amplifiers.

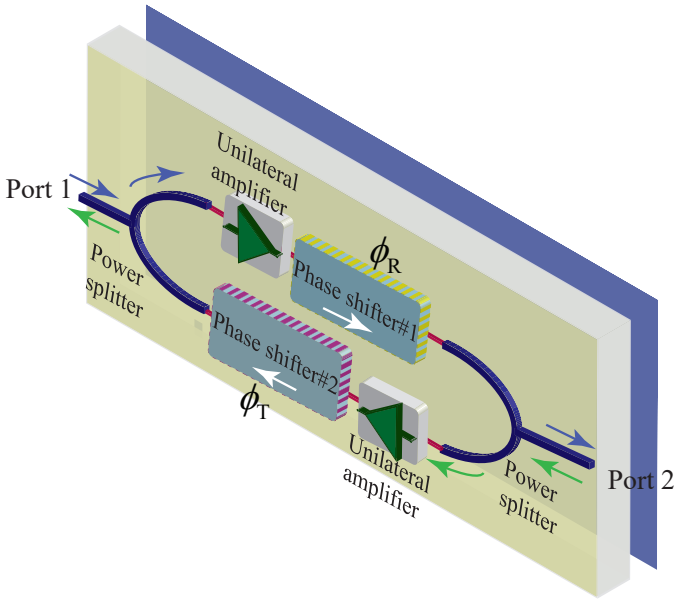

Figure 5: Two-way nonreciprocal phase shifter and amplifier composed of two amplifiers, two reciprocal phase shifters, and two power splitters.

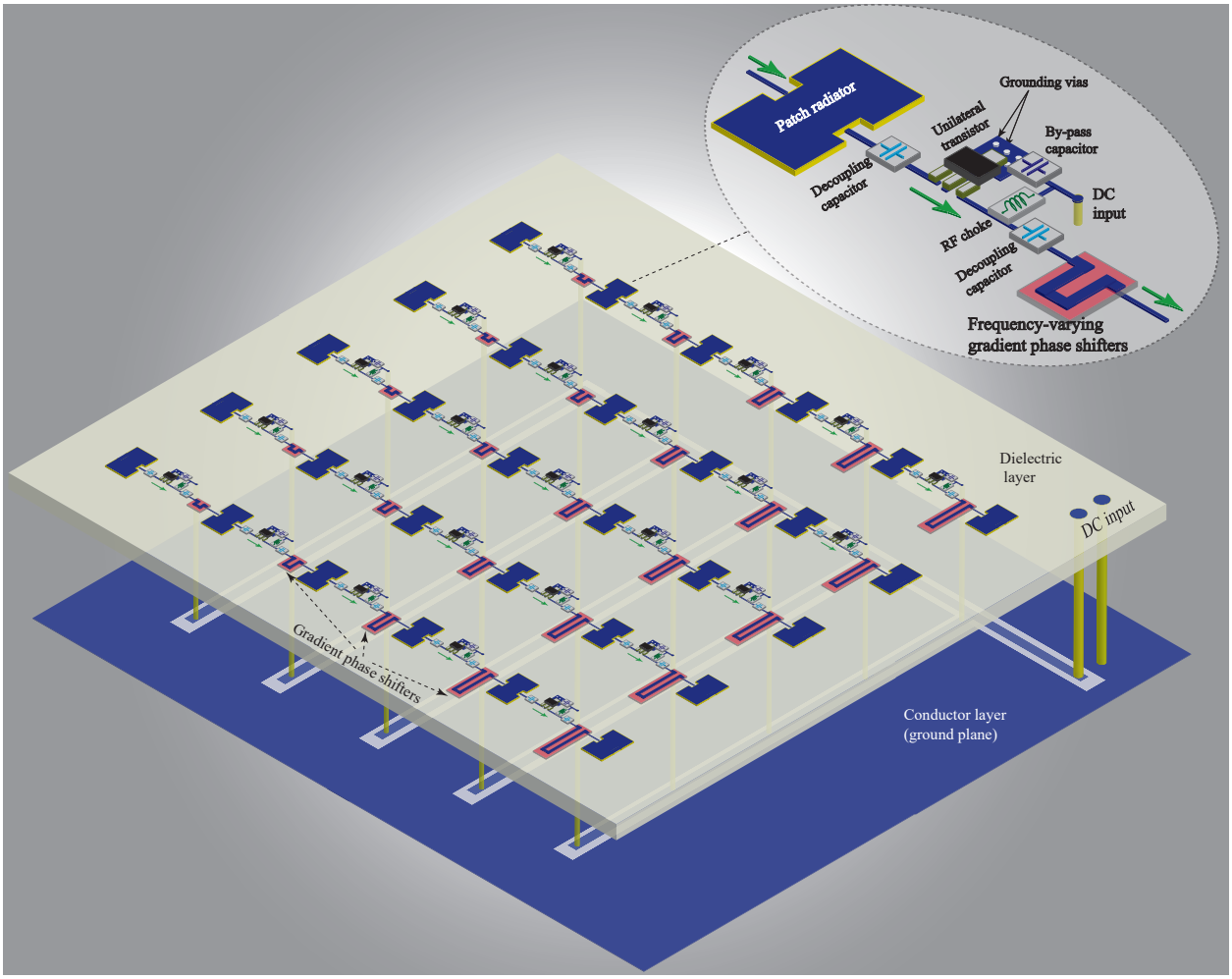

Figure 6: Architecture of the fabricated reflective beamsteering metasurface.

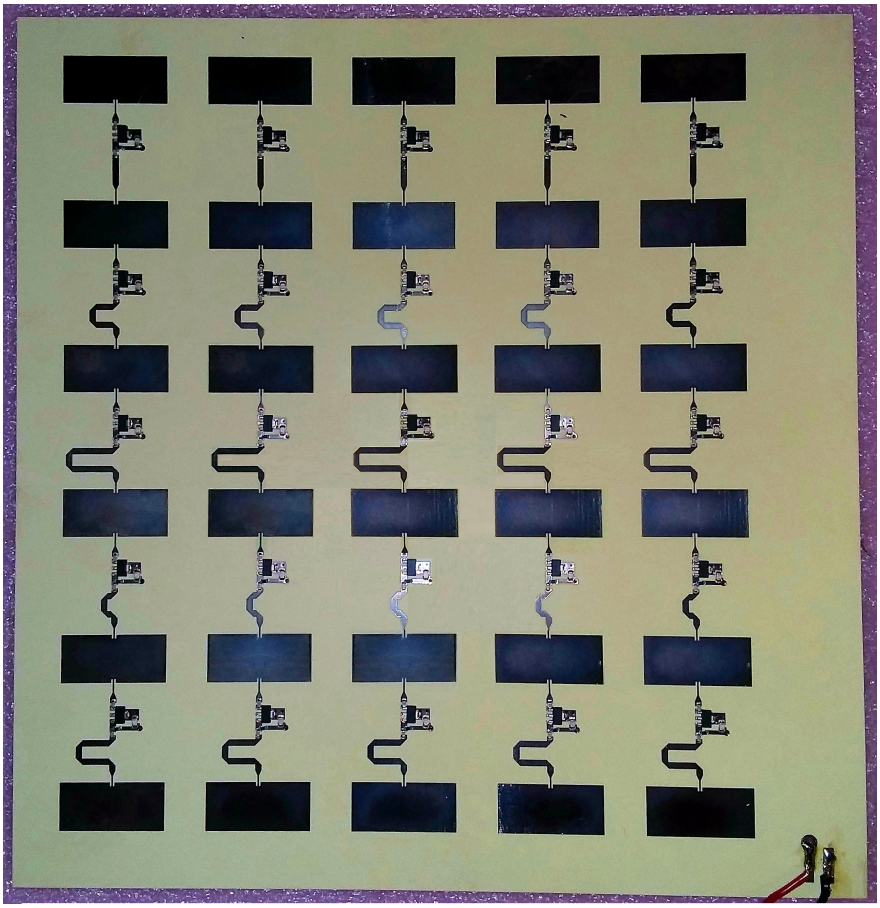

(a)

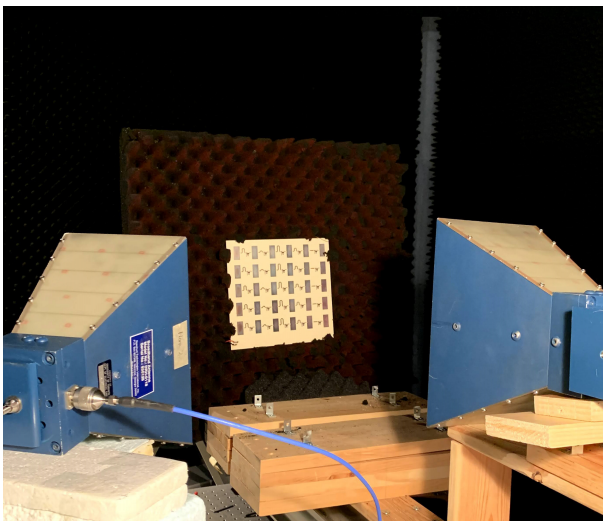

(b)

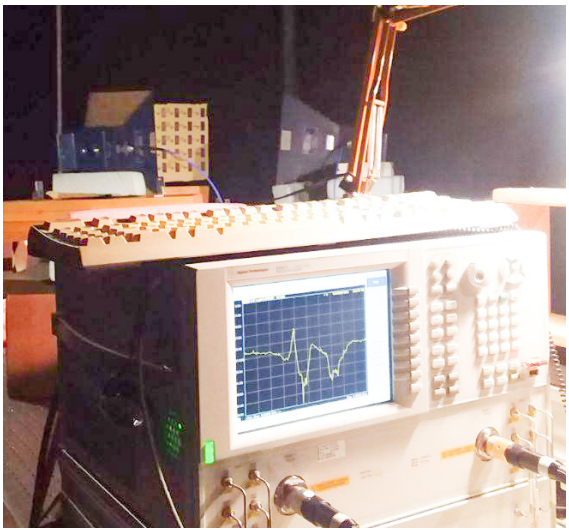

(c)

Figure 7: Experimental demonstration. (a) A photo of the fabricated metasurface. (b) and (c) Measurement set-up.

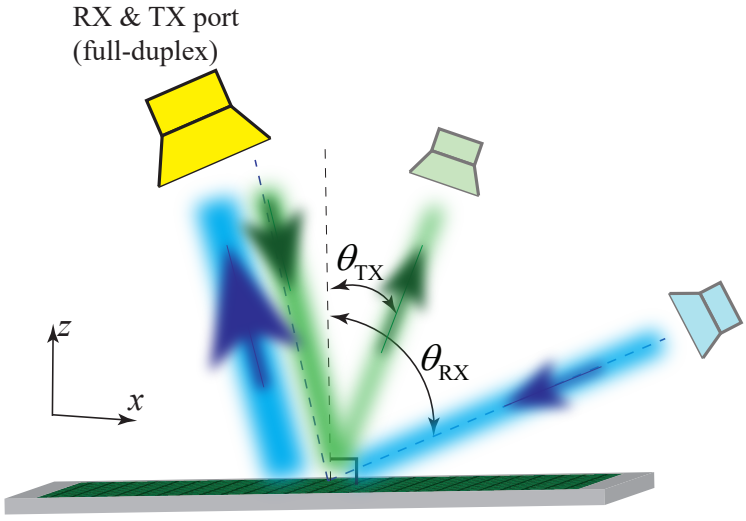

Figure 8: Full-duplex nonreciprocal-beam reflection and reception of the reflective metasurface.

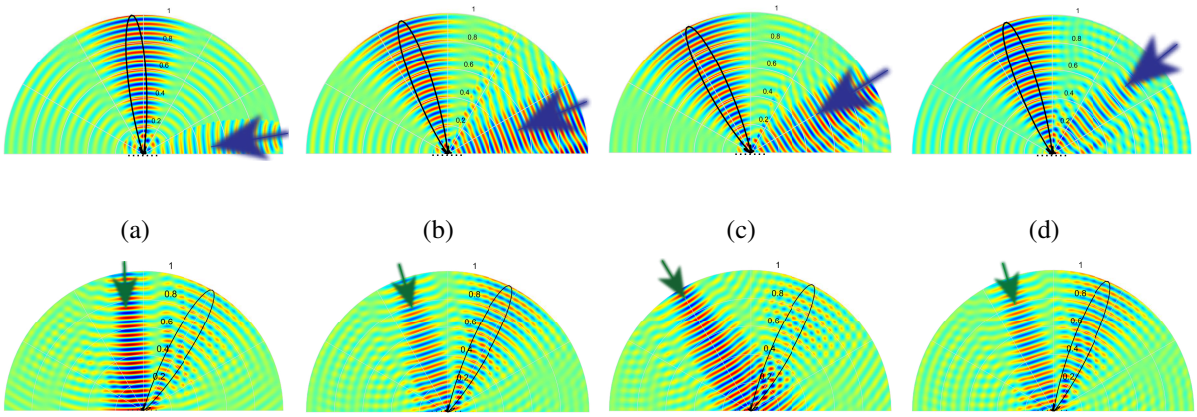

Figure 9: Full-wave simulation results for nonreciprocal reflective beamsteering for (a)-(d) forward wave incidence, and (e)-(h) backward wave incidence for nonreciprocity examination. (a) $\theta_{\mathrm{i}} = 80°$. (b) $\theta_{\mathrm{i}} = 70°$. (c) $\theta_{\mathrm{i}} = 60°$. (d) $\theta_{\mathrm{i}} = 50°$. (e) $\theta_{\mathrm{i}} = -5°$. (f) $\theta_{\mathrm{i}} = -20°$. (g) $\theta_{\mathrm{i}} = -28.5°$. (h) $\theta_{\mathrm{i}} = -20°$.

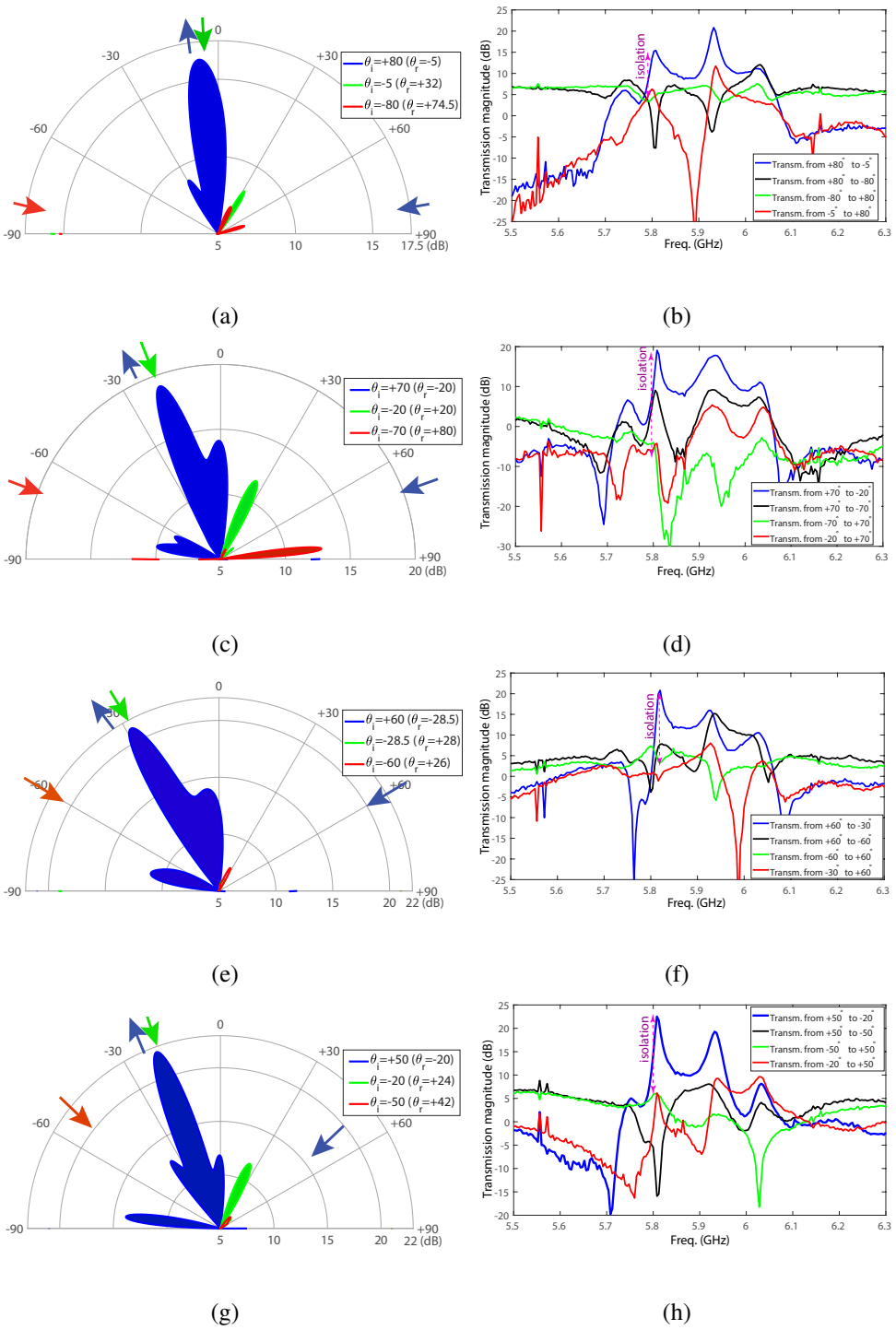

Figure 10: Experimental results for the angular and frequency responses, for wave incidence upon different angles of incidence. (a) and (b) $\theta_{\mathrm{i}} = 80°$. (c) and (d) $\theta_{\mathrm{i}} = 70°$. (e) and (f) $\theta_{\mathrm{i}} = 60°$. (g) and (h) $\theta_{\mathrm{i}} = 50°$.

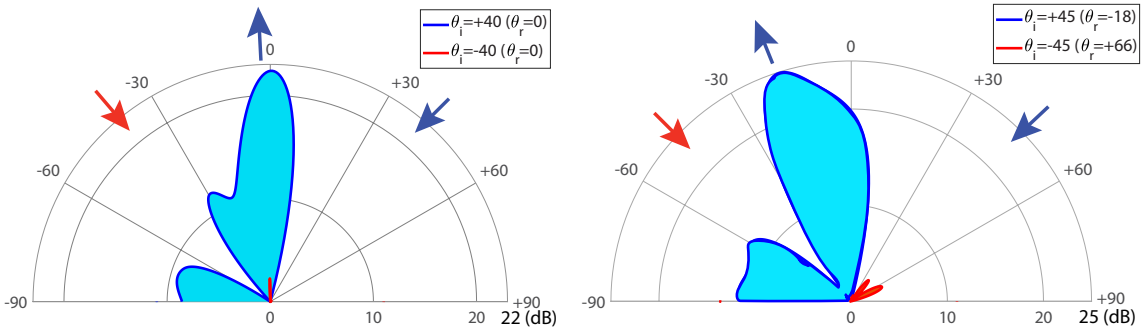

(a) (b)

Figure 11: Experimental results for nonreciprocal wave amplification. (a) $\theta_{\mathrm{i}} = 40°$. (b) $\theta_{\mathrm{i}} = 45°$.

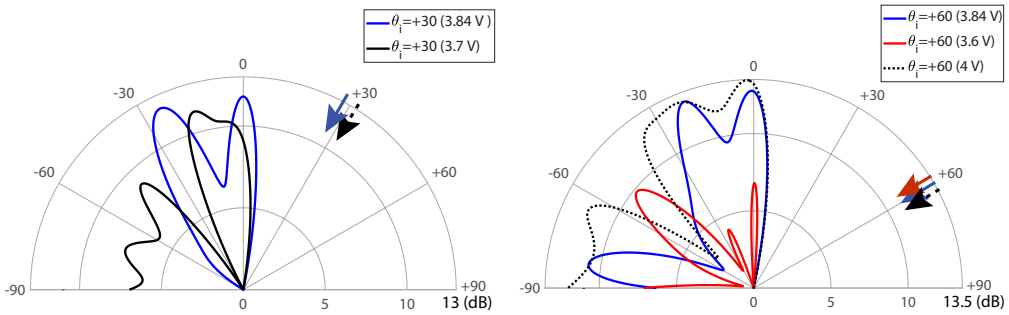

(a) (b)

Figure 12: Experimental results for the programmable and controllable beamsteering mechanism via adjustment of the DC bias of the transistors, for wave incidence upon the angle of incidence (a) $\theta_{\mathrm{i}} = 30°$. (b) $\theta_{\mathrm{i}} = 60°$.

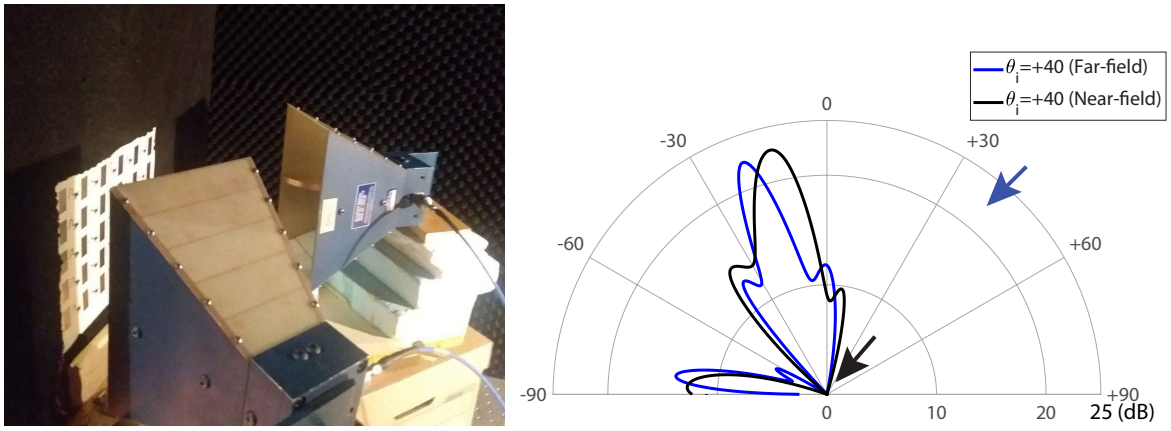

(a) (b)

Figure 13: Experimental results for near-field efficiency of the reflective metasurface. (a) A photo of the near-field experimental set-up. (b) Near-field beam versus far-field beam of the metasurface for wave incidence upon the angle of incidence $\theta_{\mathrm{i}} = 40°$.

Table 1: Full-duplex nonreciprocal reflective beamsteering at 5.81 GHz.

1	2	3	4	5	6	7
Forward incidence angle	$+40°$	$+45°$	$+50°$	$+60°$	$+70°$	$+80°$
Forward reflection angle	$0°$	$-18°$	$-20°$	$-28.5°$	$-20°$	$-5°$
Backward incidence angle	$-40°$	$-45°$	$-50°$	$-60°$	$-70°$	$-80°$
Backward reflection angle	$0°$	$+66°$	$+42°$	$+26°$	$+80°$	$+74.5°$
Isolation level	$> 19dB$	$> 22dB$	$> 15dB$	$> 21dB$	$> 6dB$	$> 10dB$
Forward amplification level	$> 21.5dB$	$> 25dB$	$> 21.5dB$	$> 21dB$	$> 19dB$	$> 16dB$

Figures

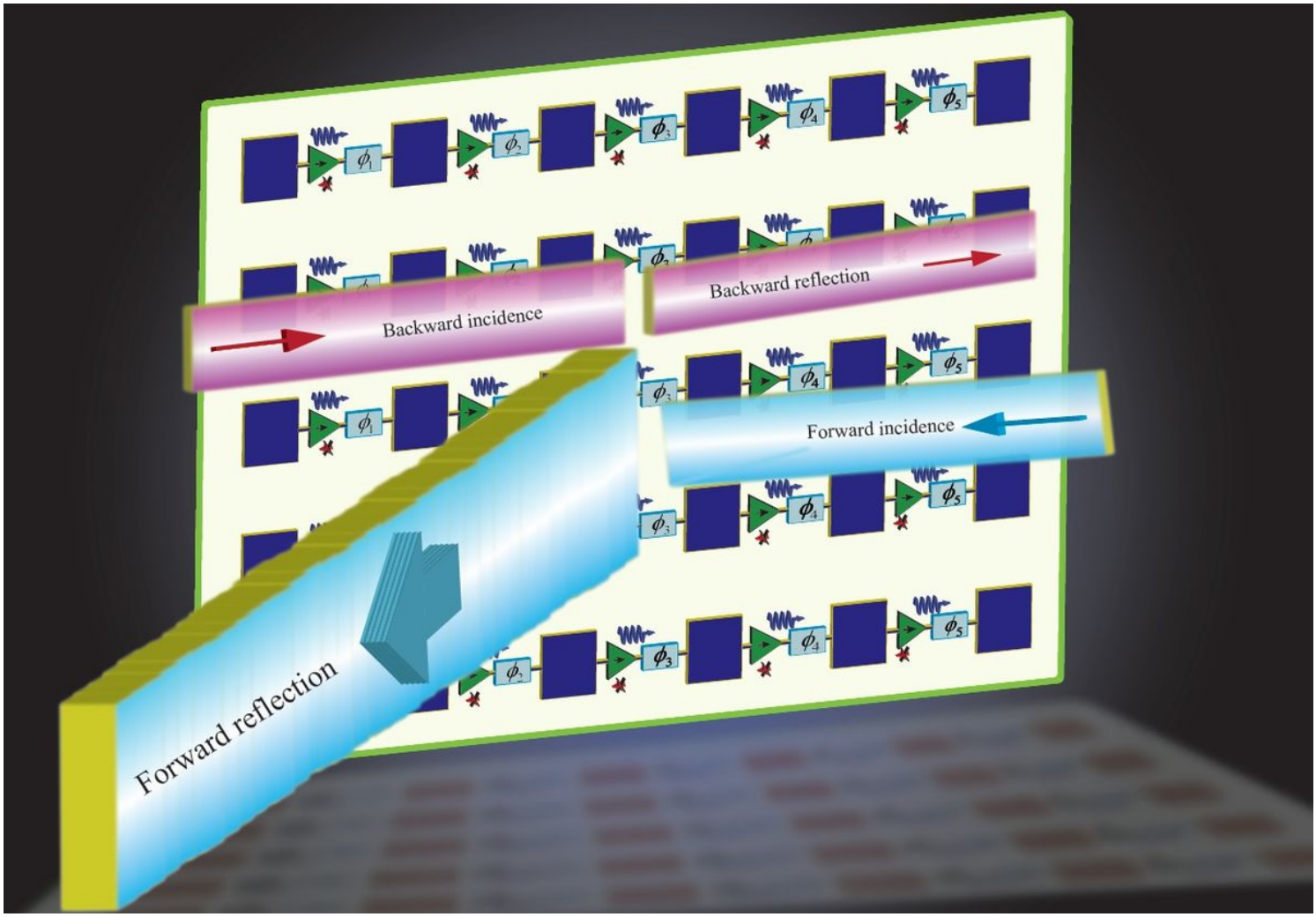

Figure 1

Schematic of the reflective beamsteering metasurface constituted of cascaded radiatoramplifier-phaser chains for simultaneous reflection and reception at different angles of reception and reflection.

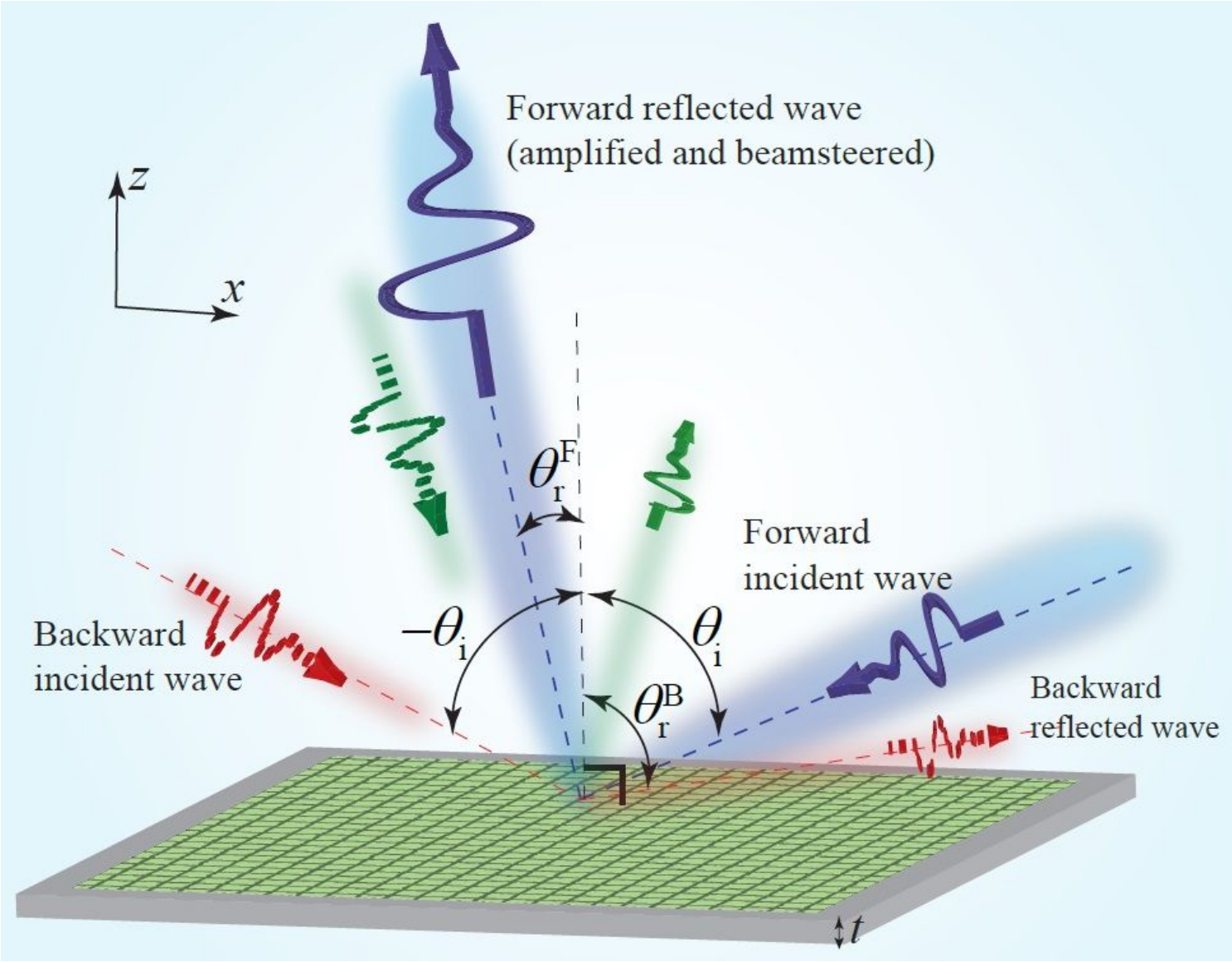

Figure 2

Functionality of the proposed reflective beamsteering metasurface.

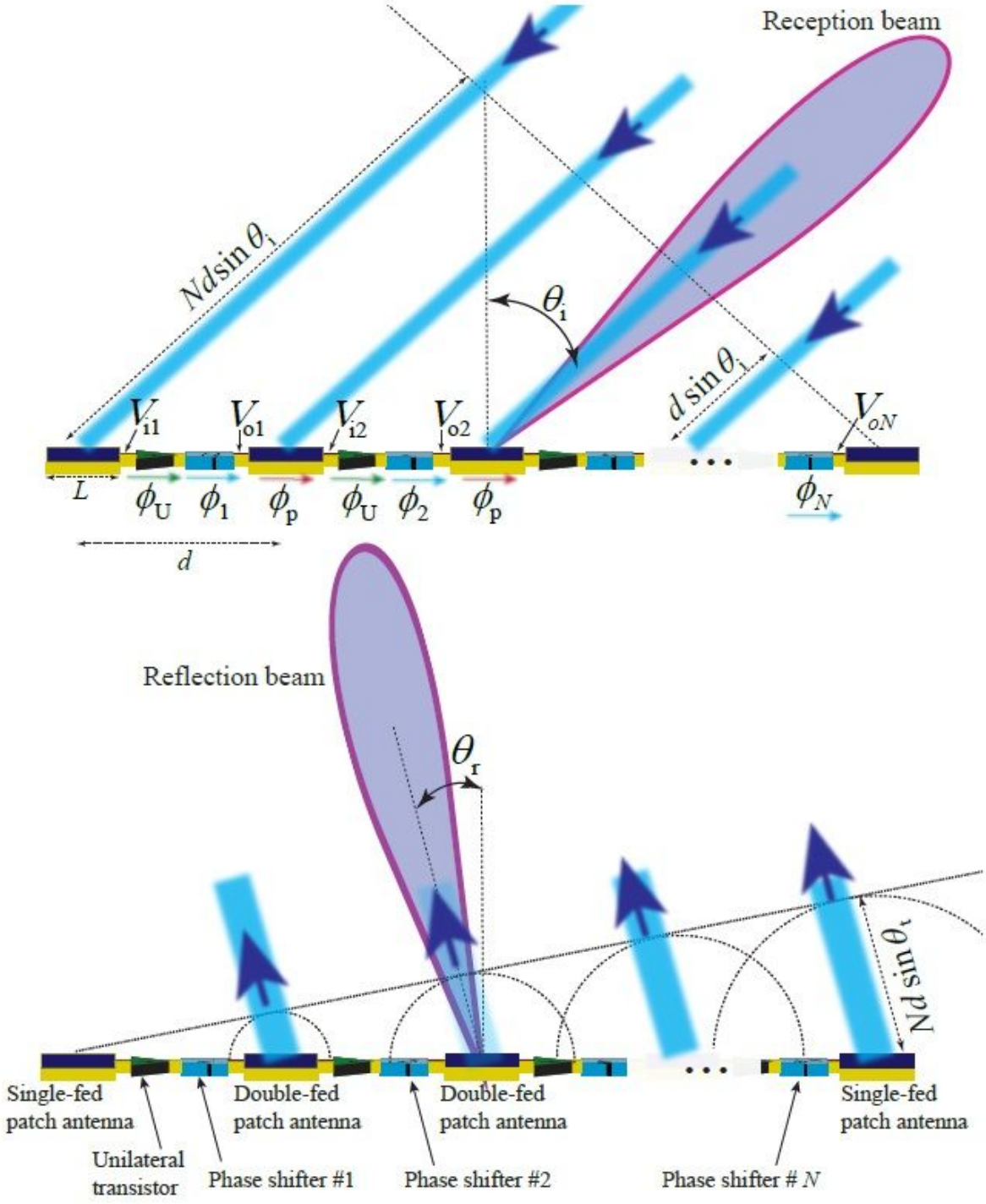

Figure 3

Beamsteering mechanism of the nonreciprocal reflective metasurface. A chain of series cascade radiating patches are integrated with nonmagnetic nonreciprocal phase shifters, providing an efficient mechanism for wave reception, one-way signal amplification, nonmagnetic nonreciprocal phase shifting and steerable wave reflection.

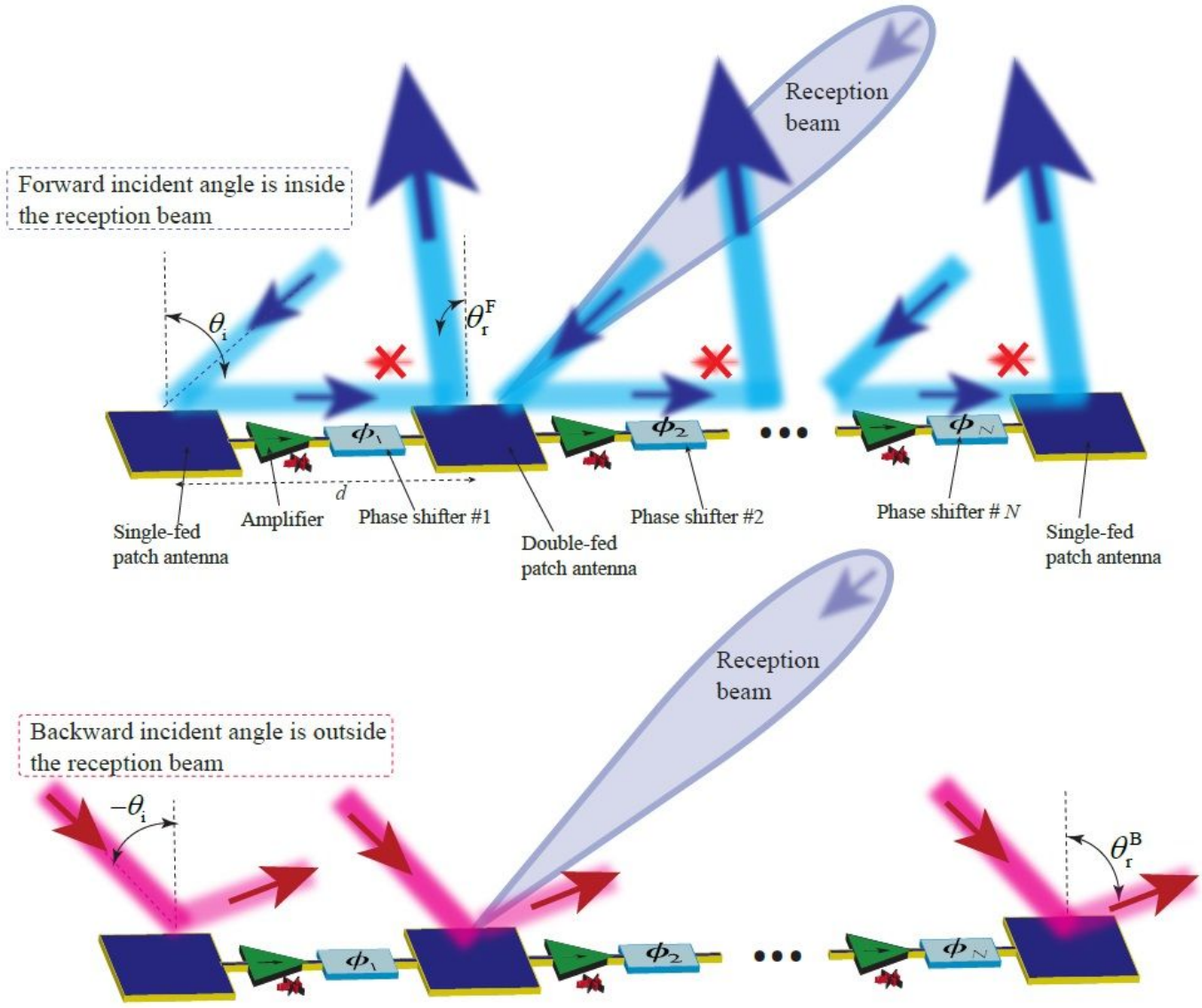

Figure 4

Nonreciprocity of the full-duplex reflective metasurface with an asymmetric reception beam governed by chains of series cascaded radiating patches integrated with phase shifters and unilateral amplifiers.

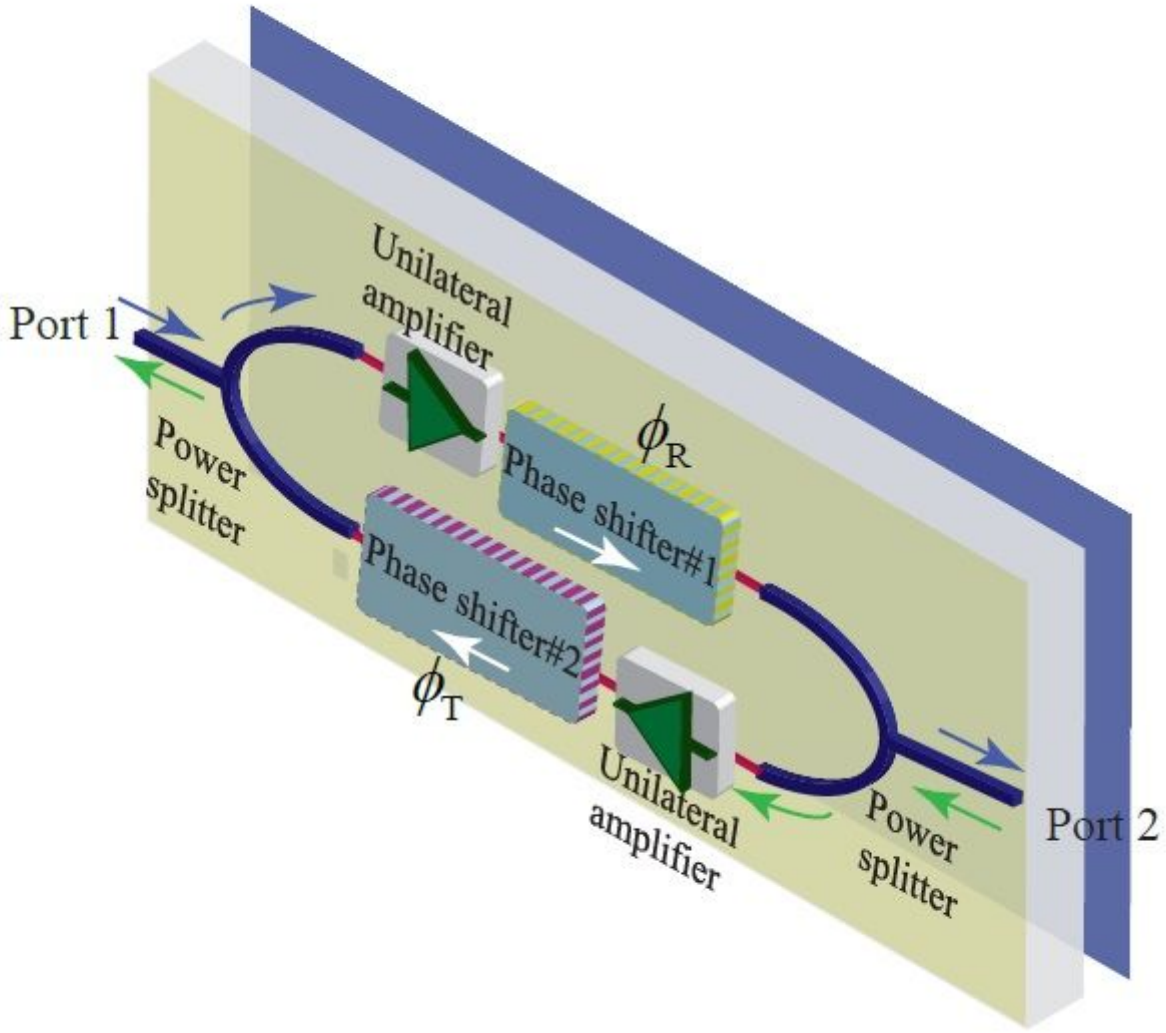

Figure 5

Two-way nonreciprocal phase shifter and amplifier composed of two amplifiers, two reciprocal phase shifters, and two power splitters.

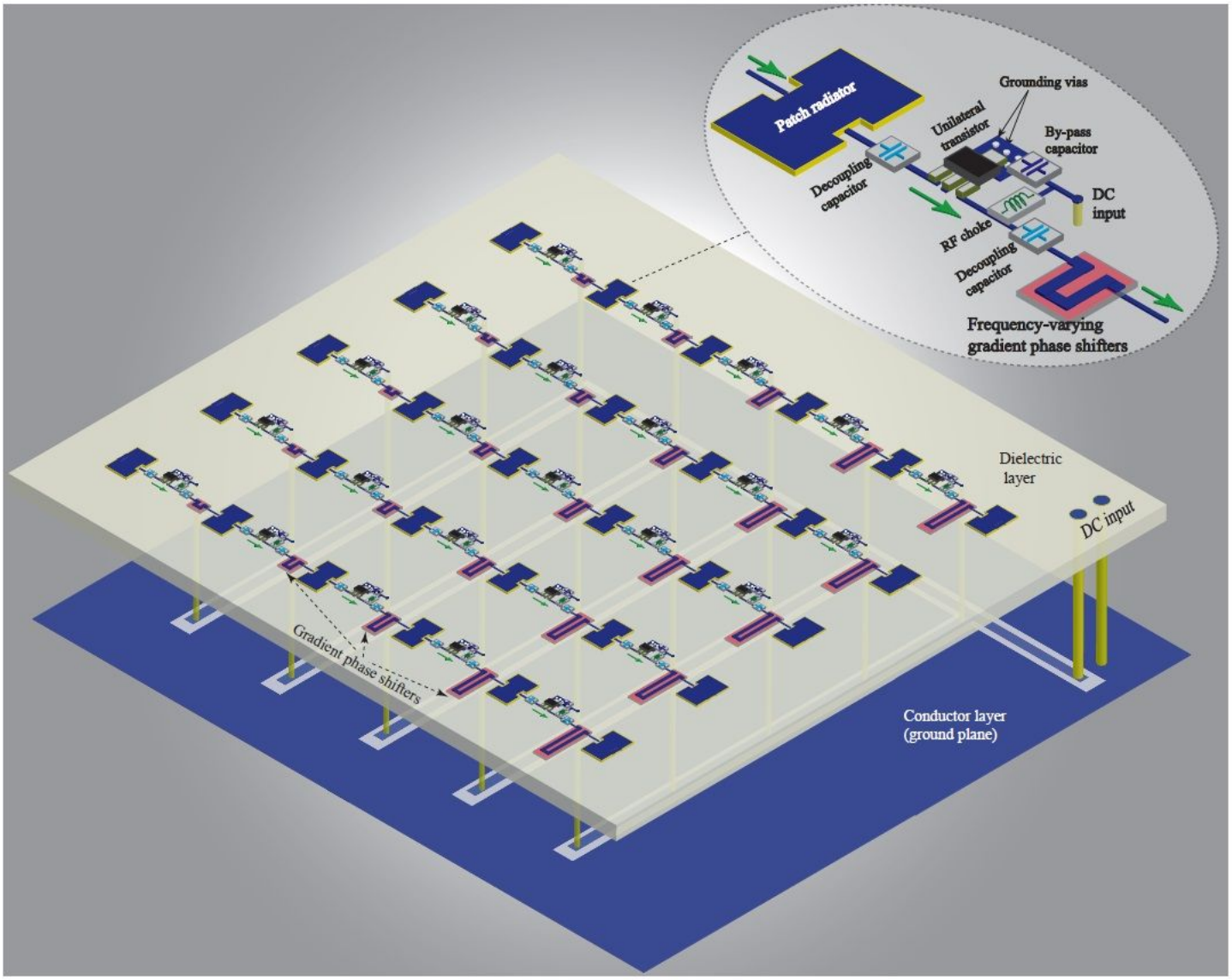

Figure 6

Architecture of the fabricated reflective beamsteering metasurface.

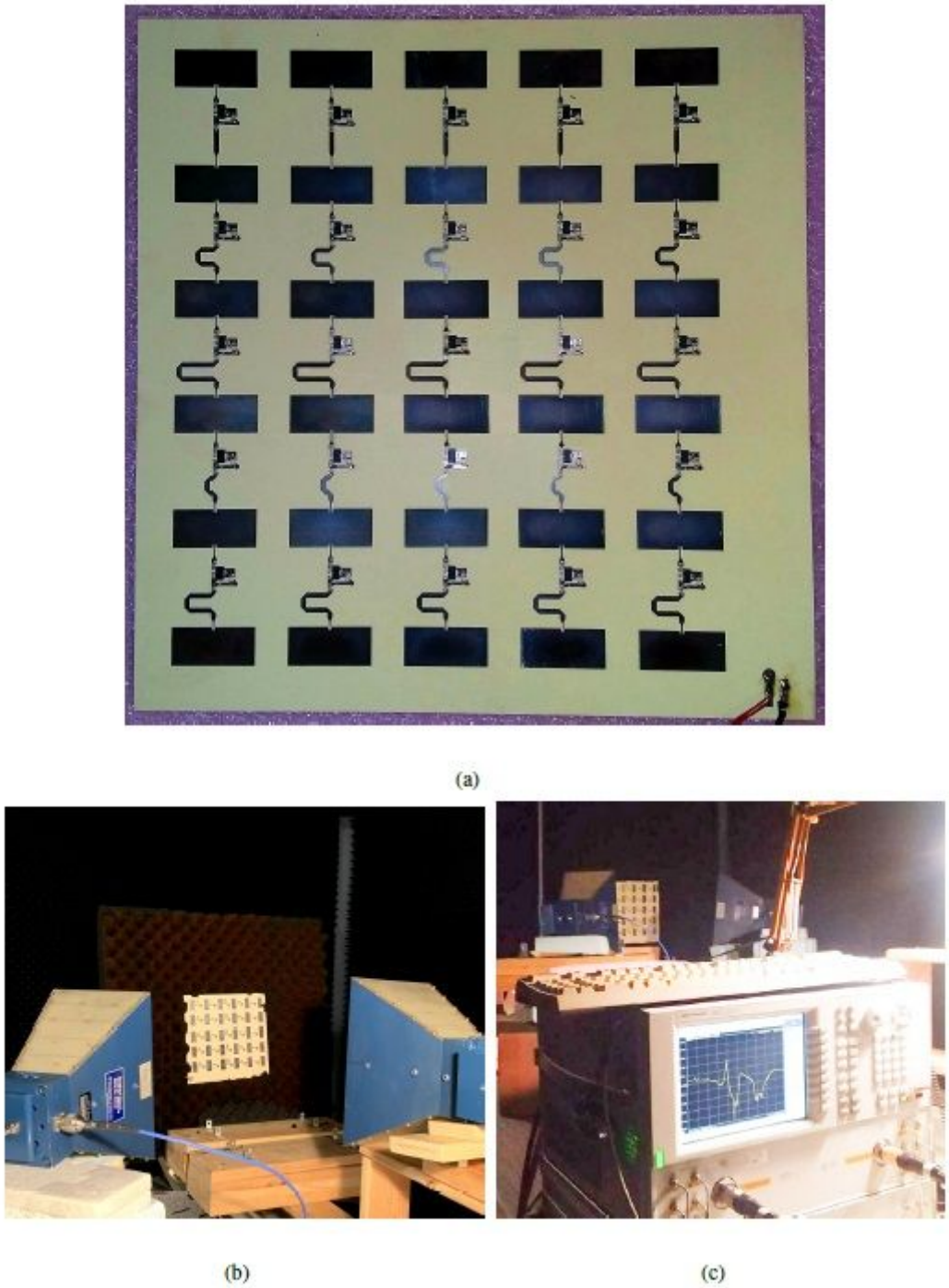

Figure 7

Experimental demonstration. (a) A photo of the fabricated metasurface. (b) and (c) Measurement set-up.

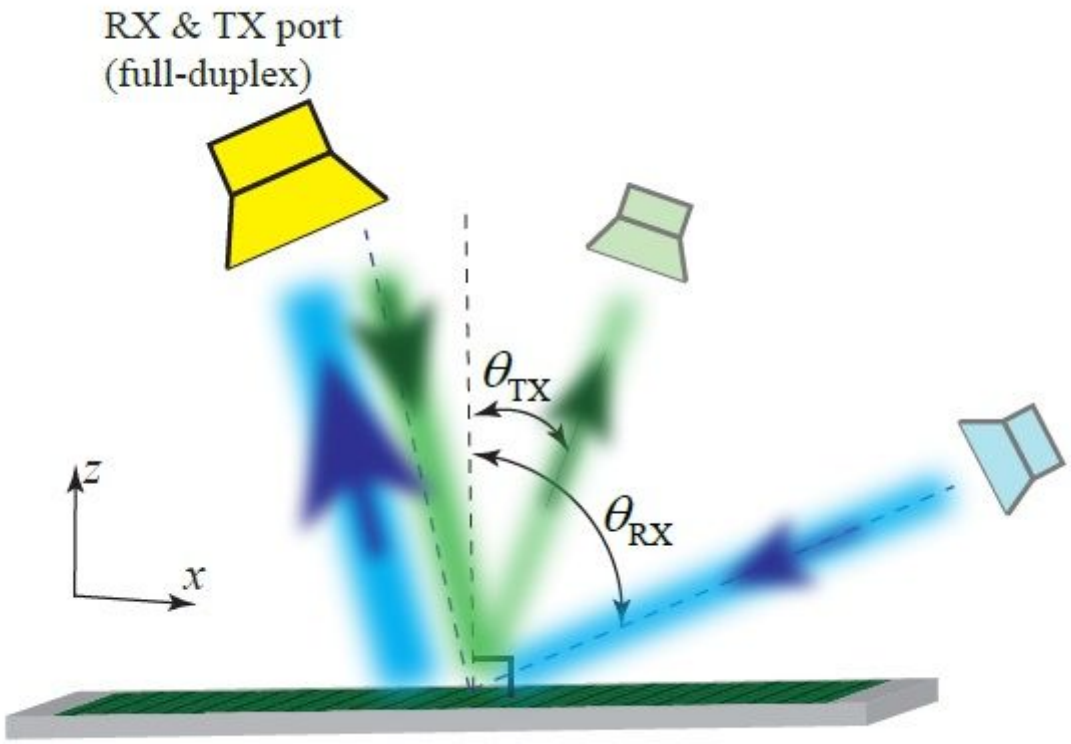

Figure 8

Full-duplex nonreciprocal-beam reflection and reception of the reflective metasurface.

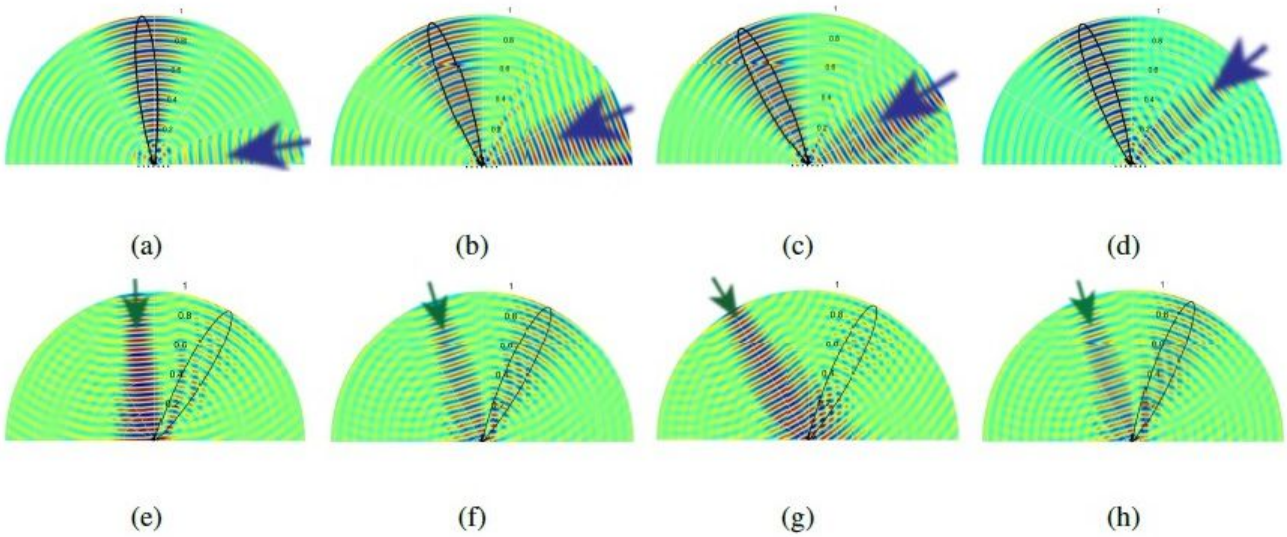

(a) $\theta_{\mathrm{i}} = 80°$.

(b) $\theta_{\mathrm{i}} = 70°$. (c) $\theta_{\mathrm{i}} = 60°$. (d) $\theta_{\mathrm{i}} = 50°$. (e) $\theta_{\mathrm{i}} = -5°$. (f) $\theta_{\mathrm{i}} = -20°$. (g) $\theta_{\mathrm{i}} = -28.5°$. (h) $\theta_{\mathrm{i}} = -20°$.

Figure 9

Full-wave simulation results for nonreciprocal reflective beamsteering for (a)-(d) forward wave incidence, and (e)-(h) backward wave incidence for nonreciprocity examination.

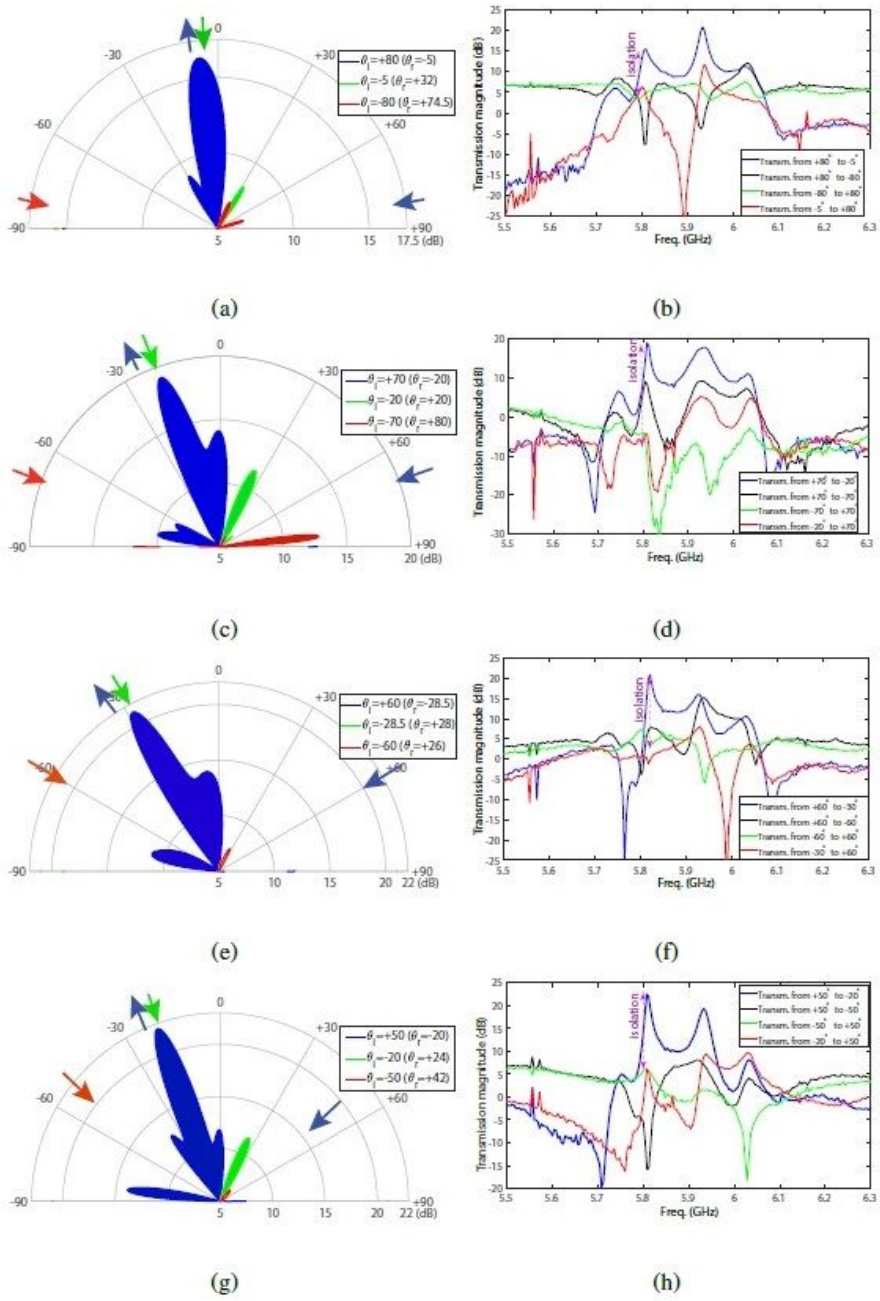

(a) and (b) $\theta_{\mathrm{i}} = 80°$. (c) and (d) $\theta_{\mathrm{i}} = 70°$. (e) and (f) $\theta_{\mathrm{i}} = 60°$. (g) and (h) $\theta_{\mathrm{i}} = 50°$.

Figure 10

Experimental results for the angular and frequency responses, for wave incidence upon different angles of incidence.

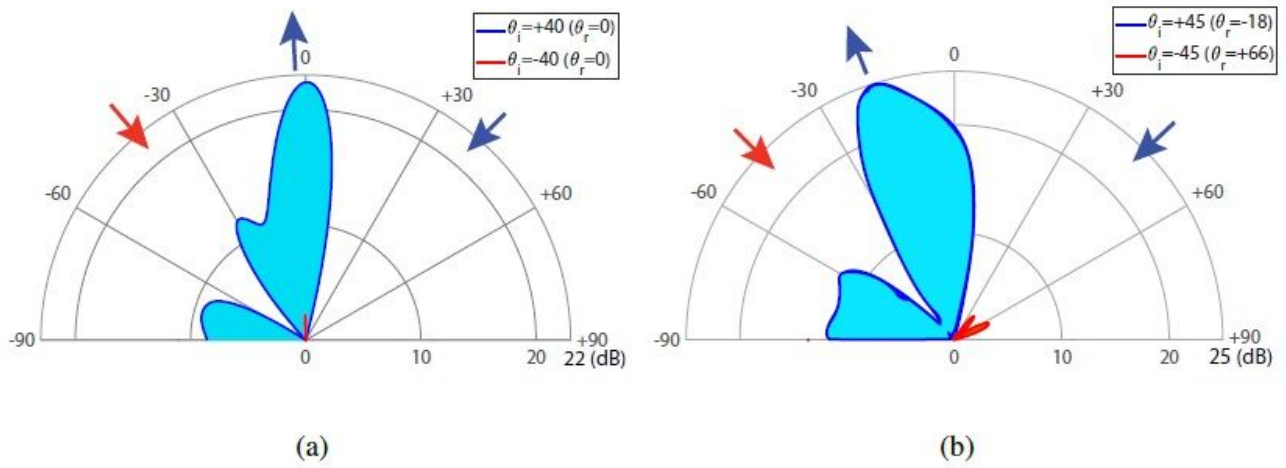

(a) $\theta_i = 40°$. (b) $\theta_i = 45°$.

Figure 11

Experimental results for nonreciprocal wave amplification.

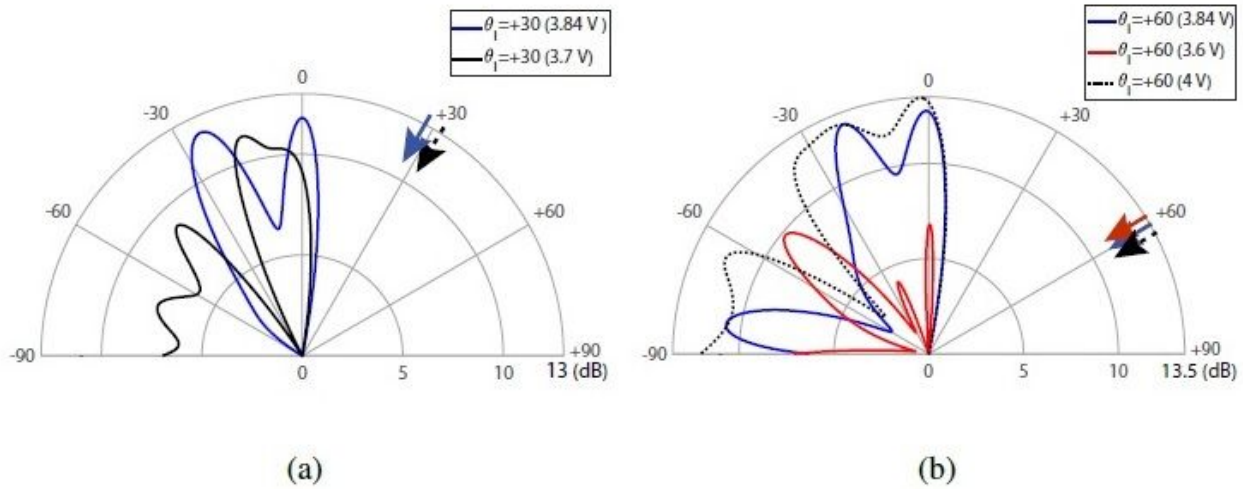

(a) $\theta_i = 30°$. (b) $\theta_i = 60°$.

Figure 12

Experimental results for the programmable and controllable beamsteering mechanism via adjustment of the DC bias of the transistors, for wave incidence upon the angle of incidence

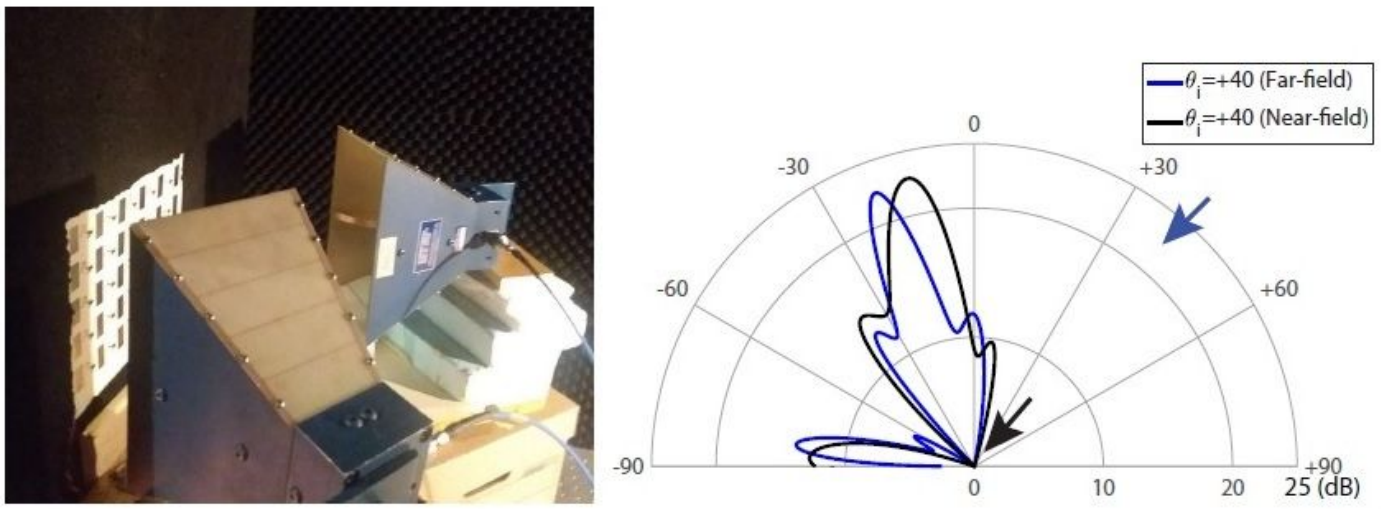

(a) (b)

$$\theta_i = 40^\circ.$$

Figure 13

Experimental results for near-field efficiency of the reflective metasurface. (a) A photo of the near-field experimental set-up. (b) Near-field beam versus far-field beam of the metasurface for wave incidence upon the angle of incidence